Computational Study of Random Boron-Carbon-Nitrogen Systems

By

SIFISO MUSA NKAMBULE

A dissertation submitted to the Faculty of Science,

University of the Witwatersrand,

In fulfillment of the requirements for the degree of Master of Science.

School of Physics,

and DST-NRF Centre of Excellence in Strong Materials,

University of the Witwatersrand,

Johannesburg,

South Africa.

2010

Declaration

I declare that this dissertation is my own work. It is being submitted for the degree of Master of Science in the University of the Witwatersrand, Johannesburg. It has not been submitted before for any degree or examination in any other university.

Sifiso Musa Nkambule:..... Date:.....2010

Acknowledgements

Firstly I would like to thank my supervisor, Professor J.E. Lowther for giving me an opportunity to work under his supervision. I greatly appreciate his mentorship and courageous support which made me to believe in myself even at times when it felt impossible.

Sincere thanks to my research focus area colleagues Onyekwelu Okeke, Thabo Letsoalo, Vuyokazi Bangani, and Mahlaga Molepo for the handful contribution to my research and for the light moments of laughter we shared, which really kept me going.

I would also like to acknowledge the Dean of the Faculty of Science in the University of Swaziland, Professor M.D. Dlamini for giving me a good recommendation. I would also like to thank the people who contributed much to my high school education: Samuel Nkambule (my father), Sabelo Nkambule

(my uncle), Sabelo Dlamini, Siphosini Mazibuko and Junior Mkhabela (my spiritual brothers). I greatly appreciate the valuable contribution they have made in my life.

Special acknowledgement goes to the special people in my life, my wife Diana and my son Junior. I specially thank my wife for believing in me and her '*I know you can do it* 'statement, which made me to try harder. I thank my son for keeping me constantly in reminder that he misses me which made me to work very hard so that I can be with him.

Lastly, the financial support received from DST-NRF Centre of Excellence in Strong materials and the University of the Witwatersrand is greatly acknowledged.

!!!!!*NgeSiSwati batsi: Kwandza kwaliwa batsakatsi, akwandze lapho nitsetse khona.* !!!!!

Dedication

To my wife, Diana Bekisiwe Magagula. With love and gratitude

!!!!! *Ulubhambo lwami Mtfombeni, Gutjwa, Komtwako, Msutfu*!!!

Citation to previously published work

Portions of this work have appeared in a published article: S.M. Nkambule and J.E. Lowther, *Crystalline and random "diamond-like" boron-carbon structures*, Solid State Communications, **150**,133-136,**(2010)**. Part of this work have been presented in the South African Institute of Physics (SAIP) conference, in July 2009, Durban, South Africa, by a poster presentation, entitled; *Computational study of random Boron-Carbon systems.*

Contents

List of Tables

List of Figures

Abstract

Elastic properties, total formation energies and cell parameters of B-C structures are studied by molecular dynamics (MD) simulation. A well tested empirical Tersoff interatomic potentialfor simulation using a General Utility Lattice program (GULP). The results are compared with the available experimental results for Diamond and BC_5. The work is extended to the study of B-C-N materials. We compare with available experimental results for BN and BC_2N.

The Bulk Modulus, Shear Modulus, Young's Modulus and Elastic constants are obtained strongly implying hardness comparable to that of diamond. The Novel B-C and B-C-N material are proposed to be ultra-hard materials with different chemical and electrical properties from those of diamond and with potentially very useful application such as advanced abrasives, high temperature electronics and semiconductors.

Chapter 1

Introduction

1.1 Strong Materials

On daily basis we rely on strong materials for many applications. Materials used in manufacturing cars, aeroplanes, powerstations, spacecraft, and various power tools need to be strong enough to protect to prevent an accident. Tools of all sorts, from fork and knives, to a wide range of precision instruments used in industry and surgery, have to stand up to different degrees of heat, abrasion and pressure. There is a great gain in different sectors if there is an improvement in the quality of strong materials because efficiency increases and costs go down.

Semiconducting devices also can be greatly improved if , for instance, the temperature at which they can function is increased.

1.1.1 Hardness Properties

Hardness is defined as resistance of a material to deformation. The term can also refer to stiffness to temper, resistance to scratching, abrasion, or cutting. It is the property of a substance, which gives it the ability to resist being permanently deformed (bent, broken, or have its shape changed), when a load is applied. The greater the hardness of the substance, the greater resistance it has to deformation. Hardness is a very complex property in the sense that it is dependant on many physical properties. It depends on various parameters like pressure, temperature, impurities, porosity, dislocations and other defects. However, it is correlated to various physical properties including ionicity, melting point, band gap, cohesive energy, etc, and can be then studied indirectly.

The hardness of a material is measured in several ways. The simplest test for non-metals is the scratch (Mohs) test[4]. Substance A is harder than substance B if A will scratch B, but B will not scratch A. There are various

other hardness test available. These include the Rockwell hardness[5], Brinell hardness[5], Vickers[6], Knoop hardness[5] and the Shore[7] test. Only the Vicker's hardness will be described in more detail.

1.1.2 Vickers Hardness

Modern scales of hardness, such as the Vickers Hardness numbers (VHN), are based on indenter tests in which an indenter is pressed into the surface of the material and the size of the impression is measured. The Vickers hardness test was developed in 1924 by Smith and Sandland at Vickers Ltd as an alternative method to measure the hardness of materials[6]. Most often the Vickers test is much easier to use than other hardness tests since the required calculations are independent of the size of the indenter. Hence the indenter can be used for all materials irrespective of hardness. Like all common measures of hardness, the basic principle is to observe the material's ability to resist plastic deformation from a standard source. The test can be used for all metals and has one of the widest scales among hardness tests with the unit of hardness known as the Vickers Pyramid Number (HV).

1.1.3 Bulk Properties

Elastic constants:

The harmonic elastic constants represent the second derivatives of the energy density with respect to strain:

$$C_{ij} = \frac{1}{V}\left(\frac{\partial^2 U}{\partial \epsilon_i \partial \epsilon_j}\right) \tag{1.1}$$

where V, U and ϵ denotes the volume, energy and strain tensor, respectively. Hence the harmonic elastic constants describe the mechanical strength of the material with respect to deformation, Since there are 6 possible strains within the notation scheme, the elastic constant tensor is a 6 x 6 symmetric matrix. The 21 potentially independent matrix elements are usually reduced considerably by symmetry[8]. For a cubic material there are only three unique elements, namely C_{11}, C_{12}, and C_{44}.

Bulk and shear moduli:

Like the elastic constant tensor, the bulk (B) and shear (G) moduli contain information regarding the hardness of a material with respect to various types of deformation. The bulk modulus is much more easily determined experimentally, than the elastic constant tensor. At zero temperature, B is

calculated using the following equation[9]:

$$B = -V\frac{dp}{dV} = V\frac{d^2U}{dV^2} \tag{1.2}$$

where V, p, and U are the volume, pressure and energy, respectively. Cohen[9] developed a relation of the bulk modulus to the to the distance of nearest neighbour separation, for compounds which are near the centre of the periodic table. His relation was;

$$B = 1761d^{-3.5} \tag{1.3}$$

Where B is in units of GPa and d, the nearest neighbours distance, is in units of Å.

If the structure of a material is studied as a function of applied isotropic pressure, then a plot of pressure versus volume can be fitted to an equation of state, where the bulk modulus is one of the curve parameters[10]. Typically a third or fourth order Birch-Murgnahan[11] equation of state can be utilised. Also, the bulk and shear moduli are related to the elastic constant elements, but no unique definition for this transformation has been found. Hebbache[12] theoretically asserted that G is correlated to the hardness of a material, which he tested for diamond.

The bulk and shear modulus can be obtained using computational methods.

Young's moduli:

When a uniaxial tension is applied to a material then the lengthening of the material is measured according to the strain. The stress to strain ratio defines the value of the Youngs modulus for that axis[13]:

$$\varepsilon_\alpha = \frac{\sigma_{\alpha\alpha}}{\epsilon_{\alpha\alpha}} \tag{1.4}$$

Where σ denotes the stress tensor. Since a material will always increase in length under tension, the value of this quantity should always be positive[10]. The Youngs moduli in each Cartesian directions can be calculated from the elastic compliances:

$$\varepsilon_x = \frac{1}{S_{11}} \tag{1.5}$$

$$\varepsilon_y = \frac{1}{S_{22}} \tag{1.6}$$

$$\varepsilon_z = \frac{1}{S_{33}} \tag{1.7}$$

Poissons ratio:

The Poisson ratio measures the change in a material at right angles to the uniaxial stress. Hence, the Poisson ratio and Young's modulus are com-

plementary properties. It is defined as the ratio of lateral to longitudinal strain under a uniform, uniaxial stress. Assuming an isotropic medium, this property can be calculated as given below [8]:

$$\nu_\alpha(\beta) = -S_{\alpha\alpha\beta\beta}\varepsilon_\beta \tag{1.8}$$

Because most materials naturally shrink in the direction orthogonal to an applied tension this leads to mainly positive values for Poisson ratio, with a theoretical maximum of 0.5[14]. values for many materials lie in the range 0.2-0.3[10], Athough negative values are also known[14]. This quantity is also be related to the bulk modulus in an isotropic material[8]:

$$B = \frac{1}{3}\frac{\varepsilon}{(1-2\sigma)} \tag{1.9}$$

where B, Σ and ϵ are as described above.

Calculations of bulk ground-state properties, such as lattice constants, atomic positions, bond lengths, and bulk modulus, play an important role in the physics of materials. Such calculations allow us to understand, characterize, and predict mechanical properties of materials in our surroundings, under extreme conditions, such as in geological formations and settings, and for industrial applications.

Crystalline materials occur in many different structures and, in contrast to isotropic materials, the description of the ground state of crystalline materials may in general need multiple lattice parameters and an atomic basis[15]. Owing to the cubic symmetry of the diamond structure, there are only three independent elastic constants, C_{11}, C_{12}, and C_{44}.

Cubic lattice

The cubic (or isometric) crystal system is a system where the unit cell is in the shape of a simple cube. It is the most common and simplest shapes found in crystals and minerals. There are three main varieties of these crystals called simple cubic (sc), body-centred cubic (bcc), and face-centred cubic (fcc). The lattices are shown in figure 1.1. A diamond has a fcc cubic symmetry and its primitive basis has two identical atoms[4].

Tetragonal lattice

Tetragonal crystal lattices result from stretching a cubic lattice along one of its lattice vectors, so that the cube becomes a rectangular prism with a square base (a $\times$ a) and height ($c \neq a$). There are two tetragonal Bravais lattices: the simple tetragonal (from stretching the simple-cubic lattice) and

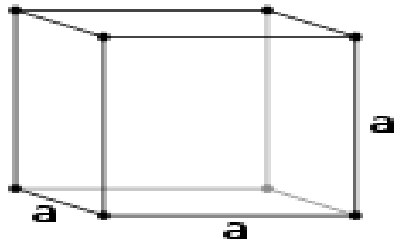

(a)

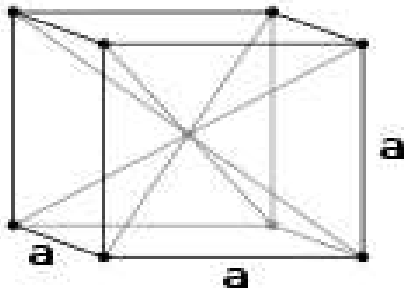

(b)

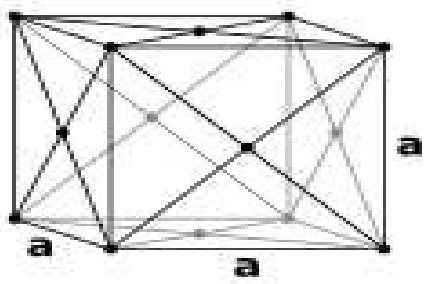

(c)

Figure 1.1: Types of cubic lattice symmetries, (a) sc, (b) bcc, (c) fcc

the centred tetragonal (from stretching either the face-centred or the body-centred cubic lattice). This is shown in figure 1.2[1].

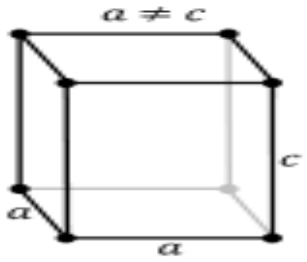

(a)

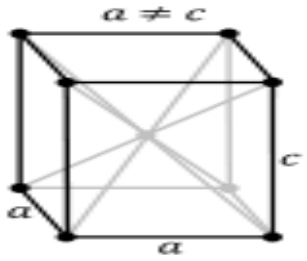

(b)

Figure 1.2: Tetragonal lattice symmetries, (a) simple tetragonal, (b) body-centred tetragonal

Trigonal lattice

The rhombohedral system can be thought of as the cubic system stretched diagonally along a plane. a = b = c; $\alpha, \beta, \gamma \neq 90°$, as shown in figure 1.3.

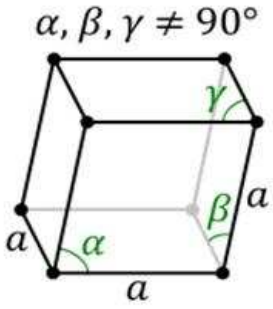

Figure 1.3: Trigonal lattice symmetries [1]

.

The tetragonal lattice can be very close to being cubic if $a \approx c$. A trigonal lattice can be almost cubic if $\alpha, \beta, \gamma \approx 90°$.

Knowledge of crystal structures of different materials at atomic level may lead to improved or new materials. These are refined with the help of computer modelling, which simulates the behaviour of the material under different conditions. This kind of fundamental work helps to indicate, for instance, what processes could be applied to create the crystal structures that, in turn, will most likely give rise to the desired properties and behaviour of the material.

1.2 Diamond

Diamond is the hardest known material with many fascinating properties. It has found a wide range of applications in modern science and technology owing to its unique properties, such as extreme hardness, high thermal conductivity, wide band gap and high electron and hole mobility[16]. It has many unique properties owing to the tetrahedrally coordinated carbon covalent bonds. The primitive basis has two identical carbon atoms. Each carbon atom has 4 nearest neighbours and 12 next nearest neighbours. Other properties of diamond include very large elastic modulus, high sound velocities, and high Debye temperature (2340 K)[17]. The carbon atoms form very short covalent bonds.

The high atomic density of diamond (1.76×10^{23} atom/cm^3) accounts for its record elastic and mechanical properties, but at the same time limits the possibilities for doping it[18].

Although there are few prospects of diamond-based microelectronics ousting silicon totally, diamond devices could function in situations when silicon electronics fail. For example, diamond chips could potentially still work at temperatures of several hundreds degrees, whereas silicon devices generally

fail above 450 K.

On the other hand diamond has some pitfalls. It is non-resistant to oxidation. While diamond stands out as the best material in cutting and polishing metals and other hard solids, its superiority fails in cutting certain tough materials such as ferrous metals owing to the detrimental formation of iron carbide during high-speed machining[19]. Another pitfall with diamond is that its shape can not be easily changed and it wears easily at high temperature.

Synthetic materials with a comparable hardness, are potential candidates to mitigate this limitation. There is an ever increasing demand for diamond-like materials in electronic applications. The growing demand for advanced superhard materials for cutting and shaping hard metals and ceramics, as well as in electronic and electrochemical applications, has stimulated the research for novel diamond like phases that are more thermally and chemically stable than pure diamond[16].

1.3 B-C complexies

Boron is an important impurity in diamond as a point defect[20]. It is effective in enhancing the hardness of diamond[21]. It makes the material exhibit p-type behaviour with very nearly shallow defect characteristics[22, 21]. It readily make a substitution of carbon atom in the diamond lattice about which there is very little lattice relaxation[20, 23]. The surface is the easiest place to make substitution for the carbon atoms without disturbing the strong sp^3- bonding network of the diamond lattice. Each boron atom replace a carbon atom on the diamond surface to form covalent bonds with three carbon atoms below it giving the boron 3-fold coordination. Surface boron atoms form planar sp^2 bonds with carbon atoms and the compressive stress from the underlying bulk diamond lattice reduces the bonds significantly. Bulk and shear moduli in the surface region increase substantially, surpassing those of bulk diamond[24]. However, only a very limited amount of boron (2 at%) can be introduced into diamond structure by common methods of thermal chemical vapour deposition and high pressure synthesis[20]. The limiting concentration of boron that can be incorporated into diamond structure has not been established yet, although under extreme pressure-temperature conditions, this content could be significantly increased. Since

all B-C materials show higher resistance to oxygen and ferrous metals than similar carbon materials[16], the diamond like B-C phases with high boron content are expected to combine the best properties of the elements including advanced electrical and optical properties, very high hardness, and high thermal and chemical stability.

Boron-doped diamond is a very interesting material for the investigation of impurity conductivity[25, 26, 27].This is a result of a wide temperature region of hopping conductivity and to unusual behaviour of the Hall coefficient[28].

Point defect calculations for large concentration of boron in diamond have highlighted the fact that the near-neighbour pairing of boron atoms is unlikely, suggesting that the complex is metastable[29]. However it has been suggested[30, 28, 31] that the presence of such a near-neighbour defects is deduced from the conductivity of heavily doped boron in diamond. The discovery of superconductivity[32] following extreme conditions of high pressure treatment further suggest this near-neighbour pairing. Recent studies[33] suggest that the near-neighbour boron (B) pairs may be formed in diamond and even act as traps for hydrogen, implying that large concentration of boron can be induced into diamond, however in a metastable form. Metasta-

bility is further implied by the fact that extreme conditions are apparently a prerequisite for the synthesis of diamond in which superconductivity has been found.

A typical amount of boron to be doped in diamond that has been successfully attained is $10^{17} - 10^{21} atoms/cm^3$[34, 35, 36, 37]. Boron doping causes a diamond to exhibit semiconducting properties, until, at a critical concentration of $n_B \approx 10^{20} atom/cm^3$ the doping results in a metallic-type conductivity at a moderate temperatures [38, 39]. Ekimov *et al* have pointed out that a further increase in boron concentration to $n_B \approx 10^{21} atom/cm^3$ produces superconductivity in diamond[40] ,in which the boron concentration gives the upper limit of the carrier (hole) concentration.

The latest research on the dynamics of the boron-doped diamond lattice by Raman spectroscopy[36, 41] and inelastic x-ray scattering[42] as well as the study of the critical temperature dependence of the doping level[43] indicate some advances in the experimental study of superconducting diamond.

Recently BC_5, the diamondlike B-C phase with highest boron content ever achieved has been synthesised[16]. It was found to have low compressibility

(bulk modulus of 335 GPa), to be conductive, to exhibit extreme Vickers hardness of 71 GPa and high thermal stability (up to 1900K). This makes it an exceptional superbrasive and a promising material for high temperature electronics.

A study by Brazhkin *et al*[18] shows an abnormally high thermal expansion coefficient for heavily boron-doped diamonds, which could be related to the softening of the phonon spectrum due to the formation of the soft regions located near boron atoms. It further shows that the concentration dependence of the thermal expansion coefficient suggests two different modes of B incorporation, substitutional at low doping levels and aggregation-type at higher concentrations of the B dopant.

In our study we look into 6 different structures of the B-C system, in relation to the boron concentration. We study cubic structures, which contain eight atom unit cells of $B_{4-x}C_{4+x}$,$(x = 0 \ldots 4)$. BC_3 structures are examined and two structures are considered, trigonal $(BC_3 - a)$ and tetragonal$(BC_3 - b))$, whose departure from cubic symmetry is very small. Our focus is to examine the elastic properties of each material.

1.4 B-C-N complexies

Extensive theoretical and experimental effort has been employed in finding the possibility of new low-compressibility materials with bulk modulus and hardness that is comparable to that of diamond. Ternary boron-carbon-nitride (B-C-N)compounds have attracted much attention due to their potential physical and chemical properties. B-C-N compounds have been of great interest to material scientists since the prediction of superhard $\beta - C_3N_4$[44] compound. Diamond like B-C-N compounds can be used as super-hard materials and high temperature semiconductors[45]. Carbon, nitrogen and boron in their strong covalent bonding configuration have an unusually high hardness and wear resistance and they have been widely used as coating materials[24].

Nitrogen and Boron atoms can be incorporated into the diamond lattice fairly easily[46]. Nitrogen and boron are very important impurities in diamond. Boron atoms become acceptor impurities while nitrogen atoms become donor impurities[28]. Furthermore, if nitrogen or boron atoms are used to replace surface carbon atoms on the diamond (111) surface, each N or B atom forms covalent bonds with three carbon atoms below it and such a

bonding environment is compatible with the tendency of N or B to have 3-fold coordination[47]. Substitutional nitrogen, in the diamond structure, yields a deep donor level resulting from the localization of the unpaired electron on a carbon dangling bond[48].

Considerable efforts have been devoted to the synthesis of the B-C-N compounds with different stoichiometric compositions such as BC_2N, BC_4N, and BC_6N, and with different structures such as the hexagonal and cubic structures[49, 50, 51, 52, 53].

Since Diamond and cubic Boron Nitride ($c-BN$) are well known materials exhibiting outstanding properties such as high hardness, melting point, and bulk modulus, a ternary system of cubic B-C-N, is expected to be another superhard material and to show high thermal and chemical stability. Zhao*et al* have highlighted that $c - BC_2N$ has a higher Vickers hardness (70 GPa) than $c - BN$ (45-50 GPa)[54].

Extensive experimental work has been done in the study of B-C-N comp onds. Solozhenko *et al*[55] obtained a bulk modulus of 282±15 GPa for $c-BC_2N$ using traditional axial x-ray diffraction (AXRD) under quasihydro-

static compression to 30 GPa. Employing a pressure of 18 GPa, temperature of 2200 K, and a graphitic BC_2N starting material, they[55] have obtained a cubic structure that has a much lower density. The lattice constant and bulk modulus of this low-density $c-BC_2N$ are found to be about 3.642 Åand 282 GPa, respectively.

Brillouin scattering measurements on the nanocrystalline cubic phase of BC_2N have been successfully performed using the emulated platelet scattering geometry[56] and they found a bulk and shear modulus of 259±22 GPa and 238±8 GPa, respectively. Metastable complexes of diamond-structured B-C-N complexes have been established with the synthesis of the metastable BC_2N material[57].

Different computational approaches have also been employed in the study of B-C-N materials. Sun *et al*[58] used a first principle study of heterodiamond BC_2N structures and noted that all the structures are metastable. A first principle computational approach has also been applied by Luo *et al*[53] in the study of three possible configuration of wurzite BC_2N. They noted the phase stability of one of the wurzite structures as an indication that it should be experimentally more feasible to be synthesize than zinc-blende-structured

BC_2N. Azevado *et al*[59], using first principle calculations, have confirmed that the stable structure of boron ternary monolayers (BCN) is formed by increasing the number of both C-C and B-N bonds, and is independent of the unit cell size.

Claims that a B-C-N complex structured material is the second hardest material, after diamond[55], have inspired further studies of hard materials that are potentially diamond-like in structure. In this work we explore properties of cubic B-C-N structures, aiming to ascertain the claims of hardness, by studying the bulk and elastic properties of the system. We further look at the relative energies.

In our work we consider trends in the B-C-N system. Each trend is simulated with B and N atoms being positioned at the various lattice sites of the diamond lattice. We look at the trends of $B_4N_{4-x}C_x$, $B_{4-x}N_{4-x}C_{2x}$, and $B_{4-x}C_{4+x}$, ($x = 0 \ldots 4.$). The approach considers both crystalline and random structures and in order to do this we use a bond order potential formalism employing the Tersoff approach[60, 61].

Chapter 2

Computational Details

2.1 Potential Functions

A molecular dynamics simulation requires the definition of a potential function, or a description of the terms by which the particles in the simulation will interact[62]. Molecular interactions are classified as *intra-atomic* or *interatomic*[63]. Examples of intramolecular potential functions include bond potentials, distance restraints, valence angle potentials, and dihedral angle potentials, where they are defined by a vector r_{ij} between two atoms i and j as shown in the figure 2.1[2].

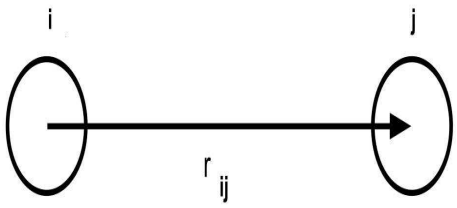

Figure 2.1: The interatomic bond vector[2].

2.2 Interatomic potentials

Interatomic potentials are potentials that involve more than one body. An important distinction between these and intramolecular (bonded) forces is that they are mainly specified by atom types rather than atom indices[2, 64]. examples of intermolecular interactions include Buckingham, Lennard-Jones, Stillinger-Weber, Axilrod-Teller[65] and the Tersoff potential[66] which is of particular interest to our study.

2.2.1 Tersoff potential

The Tersoff potential is a density dependent potential, which has been designed to reproduce the properties of covalent bonding in systems containing carbon, silicon, germanium and their compounds of these elements[67, 2, 61, 68]. Tersoff[68] developed a pair potential whose strength depends on

the environment. This idea is similar to that of the "glue model" in metals, which uses the coordination of the atom as the variable controlling the energy[69]. This potential allows bond breaking and associated changes in bond hybridisation and it has 11 atomic and 2 bi-atomic parameters[2].

The Tersoff potential is a bond-order potential and it is composed of a two-body expansion which depends on the local environment[70]. E, the total energy is computed by summing the energy of site i (E_i) over all n atoms; where

$$E = \sum_{i=1}^{n} E_i = \frac{1}{2} \sum_{i=1, i \neq j}^{n} U_{ij} \tag{2.1}$$

Where the term U_{ij} represents the interaction energy between atoms i and j and is a combination of repulsive and attractive terms[68].

$$U_{ij} = f_c(r_{ij})[f_R(r_{ij}) - \gamma_{ij} f_A(r_{ij})], \tag{2.2}$$

In equation 2.2, f_R and f_A are the repulsive and attractive pair potentials, respectively[67], and they have the following form:

$$f_R(r_{ij}) = A_{ij} \exp(-a_{ij} r_{ij}), f_A(r_{ij}) = B_{ij} \exp(-b_{ij} r_{ij}) \tag{2.3}$$

The term f_c, on the other hand is the smooth cutoff function[68], which can be described as:

$$f_c(r_{ij}) = \begin{cases} 1: & \text{if } r_{ij} < R_{ij} \\ \frac{1}{2} + \frac{1}{2}\cos[\pi\frac{(r_{ij} - R_{ij})}{(r_{ij} - R_{ij)}}]: & \text{if } R_{ij} < r_{ij} < S_{ij} \\ 0: & \text{if } r_{ij} > S_{ij} \end{cases} \tag{2.4}$$

The term γ_{ij} expresses the dependence of each bond upon the local environment and is lowered when the number of neighbours is relatively high[67].

$$\gamma_{ij} = \chi_{ij}(1 + \beta_i^{\eta_i}\zeta_{ij}^{\eta_i})^{\frac{-1}{2\eta_i}} \tag{2.5}$$

The effective coordination number of atom i is defined by the term ζ_{ij}[2],where;

$$\zeta_{ij} = \sum_{k \neq i,j} f_C(r_{ik})\omega_{ijk}g(\theta_{ijk}) \tag{2.6}$$

θ_{ijk} here defines the bond angle between the vector r_{ij} and r_{ik}, as shown in figure 2.2.1. , and θ_{ijk} can be further computed as [3],

$$\theta_{ijk} = \{\frac{\vec{r}_{ij} \cdot \vec{r}_{ik}}{r_{ij}r_{ik}}\} \tag{2.7}$$

$$g(\theta_{ijk}) = 1 + \frac{C_i^2}{d_i^2} - \frac{c_i^2}{d_i^2 + (h - \cos\theta_{ijk})^2} \tag{2.8}$$

The function $g(\theta)$ has a minimum for $h = \cos\theta$, and the parameter d determines how sharp the dependence on the angle is, whilst c expresses the

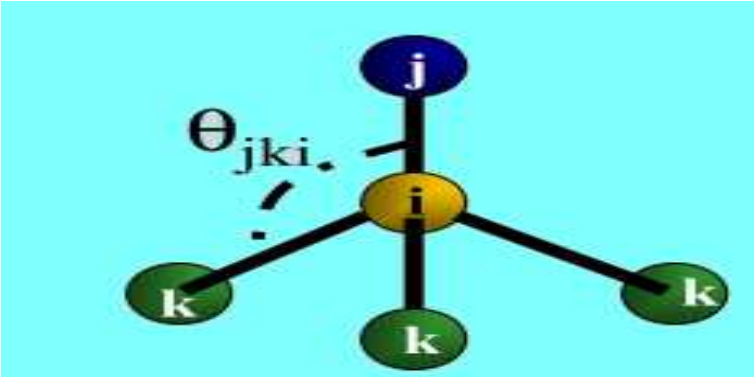

Figure 2.2: A schematic diagram showing the bond angle θ[3].

strength of the angular effect[67]. The radial force which measures the resistance to stretch[3], is represented by the term ω, which can be expressed as;

$$\omega_{ijk} = \exp^{[\lambda^3(r_{ij}-r_{jk})^3]} \tag{2.9}$$

The dependence on θ_{ijk} and $r_{ij} - r_{ik}$ of the functions g and ω can be represented by the graphs of figure 2.3 and 2.4.

The further mixed parameters for a binary system can be defined as[2];

$$a_{ij} = \frac{a_i + a_j}{2}, b_{ij} = \frac{b_i + b_j}{2} \tag{2.10}$$

$$A_{ij} = (A_i A_j)^{1/2}, B_{ij} = (B_i B_j)^{1/2} \tag{2.11}$$

$$R_{ij} = (R_i R_j)^{1/2}, S_{ij} = (S_i S_j)^{1/2} \tag{2.12}$$

Here i, j, and k label the atoms in the system, r_{ij} is the length of the ij bond,

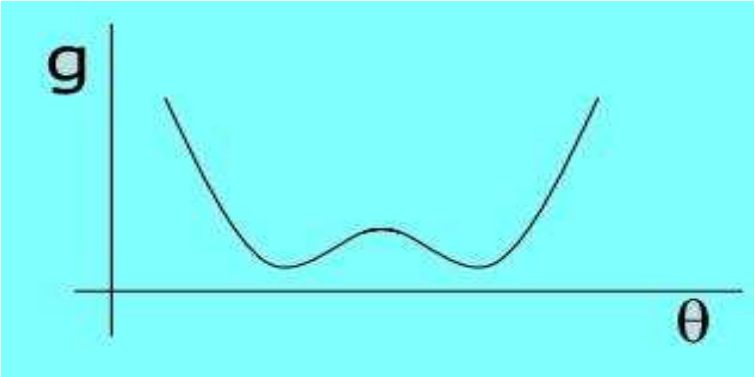

Figure 2.3: A graph showing the relationship θ and $g(\theta)$ taken from[3].

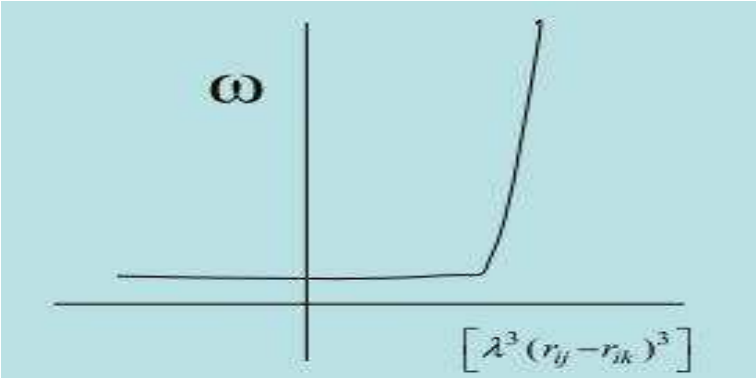

Figure 2.4: A graph showing the dependace of ω on $r_{ij} - r_{ik}$ taken from[3].

which can be calculated as;

$$r_{ij} = |r_i - r_j| \tag{2.13}$$

The 11 single subscripted parameters (e.g a_i and η_i) depend on the atom type[2].

The two sets of bi-atomic parameters, χ_{ij} and ω_{ij}, define the chemistry between different types of atoms[2]:

$$\chi_{ii} = 1,\ \chi_{ij} = \chi_{ji},\ \omega_{ii} = 1,\ \omega_{ij} = \omega_{ji} \tag{2.14}$$

The Tersoff potentials are distinctively short ranged, typically of order 3 Å[71]. These potentials have been found to give a convenient and relatively accurate description of the structural properties and energies of carbon, including elastic properties, phonons, polytypes, and defects and migration barriers in diamond and graphite [66, 72, 61, 68]. The Tersoff potentials work very well for zincblende group IV and group III-V semiconductors and their compounds [3].

2.3 Previous studies using Tersoff potentials

Studies have developed Tersoff potential parameters for C[60, 61] and B[72]. There are also two sets of N potentials developed by Matsunaga *et al*[72] and Fazzio *et al*[73]. The parameters are listed as shown in Table 2.1:

The biggest challenge of the Tersoff potentials is that the fit is difficult. With 6 functions to fit and angular terms, it is difficult to find a good parametrization[69]. Carbon,Silicon and Germanium are some of the materials that have been extensively studied[60, 70, 61] by fitting the tersoff potentials. In Table 2.2 we list the Tersoff parameters of Silicon[60, 70, 61], and germanium[61]. Using the Silicon parameters listed in Table 2.2 and nitrogen set 2 parameters in Table 2.1, de Brito Mota *et al*[70] have shown the reliability of the potentials by testing them for $a - SiN_x$ for a wide range of nitrogen content($0 < x < 5$), and the results are in agreement with available experimental data.

Tersoff[68] also developed and improved[60] the Silicon parameters and they yield excellent results for the elastic constants of silicon, when compared with experiments. He also developed parameters for germanium[61], which he used to propose an empirical potential for multicomponent systems, in

Elements	**B[72]**	**N(set1)[72, 74]**	**N(set2)[73]**	**C[60, 61]**
A(eV)	2.7702×10^2	1.10000×10^4	6.36814×10^3	1.3936×10^3 11
B(eV)	1.8349×10^2	2.1945×10^2	5.11760×10^2	3.467×10^2
λ(Å^{-1})	1.9922	5.7708	5.4367	3.4879
μ(Å^{-1})	1.5856	2.5115	2.7000	2.2119
β	1.500×10^{-6}	1.0562×10^{-1}	5.2938×10^{-3}	1.5724×10^{-7}
n	3.9929	12.4498	1.33041	0.72751
c	5.2629×10^{-1}	7.9934×10^4	2.03120×10^4	3.8049×10^4
d	1.5870×10^{-3}	1.3432×10^2	2.55103×10^1	4.384×10^0
h	0.5000	-0.9973	-0.99734	-5.62390×10^{-1}
R(Å)	1.8	2.0	1.8	1.8
S(Å)	2.1	2.3	2.1	2.1
Interactions($i-j$)	B-N	B-C	C-N	
χ_{i-j}	1.1593	1.0025	0.9685	
ω_{i-j}	1.000	1.0000	0.6381	

Table 2.1: Tersoff interatomic potential parameters for Carbon, Boron and Nitrogen

Elements	**Si[60, 70, 61]**	**Ge[61]**
A(eV)	1.8308×10^3	1.769×10^3
B(eV)	4.7114×10^2	4.1923×10^2
λ(Å^{-1})	2.4799	2.4451
μ(Å^{-1})	1.7322	1.7047
β	1.1000×10^{-6}	9.0166×10^{-7}
n	7.8734×10^{-1}	7.5627×10^{-1}
c	1.0039×10^5	1.0643×10^5
d	1.6217×10^1	1.5652×10^1
h	-5.9825^{-1}	-4.3884×10^{-1}
R(Å)	2.7	2.8
S(Å)	3.0	3.1
Interactions($i-j$)	Si-Ge	C-Si
χ_{i-j}	1.00061	0.9776

Table 2.2: Tersoff interatomic potential parameters for Silicon and Germanium

particular C-Si and Si-Ge system.

2.4 Molecular Dynamics

Computer simulations are carried out in the hope of understanding the properties of assemblies of molecules in terms of their structure and the microscopic interactions between them[75]. This approach complements conventional experiments and enables us to study materials properties that are quite difficult (or even impossible) to find in other ways[8, 64]. They allow detailed investigations and enables us to gain a deeper understanding of the relevant materials processes with the materials[76]. It represents a very convenient and reliable interface between theory and laboratory experiments and can be thought of as a "virtual experiment"[77]. Because molecular systems generally consist of a vast number of particles, it is impossible to find the properties of such complex systems analytically[8], hence the need for approximation. These accuracy of the predictions is subject to the accuracy of the model used

Computer simulations are mainly used as an intermediate between microscopic length and time scales and the macroscopic world of the laboratory[8]

and provides a guess of the interactions between molecules.

There numerous simulation techniques, such as Molecular Dynamics (MD) and Monte Carlo (MC), in addition, there are hybrid techniques which combine MD and MC[8]. In our study the MD technique is used.

MD is one of the principal tools in the theoretical study of molecules[77]. This is a computational method which simulates the time dependent behaviour of molecular systems[8]. It is a computer technique which solves numerically a multi-body problem of mechanics[67]. This is a form of computer simulation in which atoms and molecules are allowed to interact for a period of time by approximations of known physics, giving a view of the motion for the coordinates components of the N atoms in the assembly[77, 78]. Researchers[79] surmise that the molecular dynamics algorithm in most common use today may even have been known to Newton.

MD simulation circumvents the difficulty of finding an analytical solution in the complex systems by using numerical methods[80]. It solves numerically the $3N$ simultaneous equations of motion[80, 81], by using time integration algorithms (TIA). MD is a multidisciplinary method which probes the rela-

tionship between molecular structure, movement and function[77]. The basic laws and theories of MD are from mathematics, physics, and chemistry, and it employs algorithms from computer science and information technology. It was originally conceived within theoretical physics in the late 1950's[80]. MD can be applied in effectively describing the velocities and positions of atoms disrupted in a structure, as a function of time[67]. The microscopic behaviour of the system can be computed by solving differential equations of motion, from the initial position and velocity of the atoms, and the forces of interaction between them[80].

A MD simulation requires the definition of a potential function[77, 82], or a description of the terms by which the particles in the simulation will interact and is usually referred to as a force field. Those most commonly used are based classical mechanics and embody a classical treatment of particle-particle interactions that can reproduce structural and conformational changes but usually cannot reproduce chemical reactions[80]. The Born-Oppenheimer approximation[83], which states that the dynamics of electrons is so fast that they can be considered to react instantaneously to the motion of their nuclei,and hence the electron and the nuclei may be

treated separately. The nuclei may then be treated as point particles which follow classical Newtonian dynamics[77]. these are the two key factors that leads to the reduction from a fully quantum description to a classical potential. As a result the effect of the electrons is approximated as a single potential energy surface, usually representing the ground state[80].

2.4.1 Molecular Interactions

Molecular dynamics simulation consists of the numerical, step-by-step, solution of the classical equations of motion, which for a simple atomic system may be written as[62]:

$$m_i \ddot{r}_i = f_i \tag{2.15}$$

$$f_i = \frac{-\partial}{\partial r_i} U \tag{2.16}$$

For this purpose we need to be able to calculate the forces f_i acting on the atoms, and these are generally derived from a potential energy $U(r^N)$, where $r^N = (r_1, r_2, \ldots, r^N.)$ represents the complete set of $3N$ atomic coordinates.

Well known MD softwares includes:

- VASP[84]
- CASTEP[85]

- DL_ POLY[2]
- NEWTON-X[86]
- AMBER[87]
- GULP[65]
- NAMD[88]
- CHARMM[89]

The first two software packages do Quantum MD. In our work we use the General Utility Lattice Program(GULP)[65].

2.5 The Time Integration

Time integration algorithm (TIA) is the engine of MD. It is basically required to integrate the equations of motion and follow the trajectory of interacting particles[69, 78]. TIA is based on a finite difference method[90], which employs the discretization of time on a finite grid, and the distance between two consecutive points on the grid being the *time step*, Δt.

There are a range of TIA available. There is the Verlet algorithm[91], whose basic idea is to have to Taylor expansion of third order for the positions $r(t)$. One is forward, whilst the other is backward in time. The are two versions of the Verlet algorithm namely the Verlet leapfrog(LF) or Velocity Verlet(VV) versions[2]. Another algorithm is the Predictor-Corrector algorithm[92], which consist of 3 steps, namely the predictor, force evaluation and the corrector.

2.6 Long-range Interaction Algorithms

These methods compute the interaction energies of periodic systems, like crystals, particularly the electrostatic energies. These are[78]:

- Ewald summation
- Particle Mesh Ewald
- Particle-Particle Particle Mesh
- Reaction Field Method
- Central Difference method
- Euler-Cauchy Method

- Nordsieck Method for Newton's Equations

2.6.1 Ewald technique

The Ewald technique represents the most efficient solution for crystalline materials[93] and it is a well-established technique for the evaluation of electrostatic interactions which are necessary for many computer simulations. Ewald summation is a special case of the Poisson summation formula which replaces the summation of interaction energies which are in real space with an equivalent summation in Fourier space. Its advantage is rapid convergence[93].

2.7 The GULP code

Gulp is a molecular dynamics code capable of handling up to multi-thousand atoms[10]. It is designed to perform a variety of tasks based on force field methods. It is a flexible tool with great variety and diversity for simulation of solids based on interatomic potential models[65], including the Tersoff potentials. In GULP many algorithms have been embodied for the simulation of three-dimensional periodic systems[65]. It is suitable for the treatment of

both inorganic and organic systems with fully flexible molecules[10]. One of the principal applications of the program has been to the derivation of empirical potential parameters through least-squares fitting. The ability of GULP to treat multiple structures within the same run[65] is of particular use in our study.

Algorithms for symmetry-adapted energy minimisation of solids using analytical first and second derivatives have been included and implemented in GULP[65]. The new methods lead to improved computational efficiency of up to an order of magnitude over the standard algorithm which takes no account of symmetry. The largest improvement is obtained from the use of symmetry in the generation of the hessian[10]. Accelerated convergence techniques for the dispersion energy are found to be of great benefit in improving the precision at little extra computational cost, particularly when a one centre decomposition is possible or the Ewald sum weighting towards real-space is increased[65].

Energy Minimisation

As a prerequisite for any subsequent evaluation of physical properties, efficient minimisation of the energy is an essential part of the simulation of solids[65]. This normally represents the computationally most demanding stage. Gulp is is able to optimise at constant pressure or at constant volume, where the unit cell remains frozen[65].

Calculating bulk properties, GULP uses equations due to Voight, Reuss and Hill[94]. Below are the Reuss and Voight definitions, while the Hill values are defined as the average of the Reuss and Voight values:

$$B_{Voight} = \frac{1}{9}\left(C_{11} + C_{22} + C_{33} + 2(C_{12} + C_{13} + C_{23})\right) \tag{2.17}$$

$$B_{Reuss} = \left(S_{11} + S_{22} + S_{33} + 2(S_{12} + S_{13} + S_{23})\right)^{-1} \tag{2.18}$$

$$G_{Voight} = \frac{1}{15}\left(C_{11} + C_{22} + C_{33} + 3(C_{44} + C_{55} + C_{66}) - C_{12} - C_{13} - C_{23}\right) \tag{2.19}$$

$$G_{Reuss} = \frac{15}{4(S_{11} + S_{22} + S_{33} - S_{12} - S_{13} - S_{23}) + 3(S_{44} + S_{55} + S_{66})} \tag{2.20}$$

In this work we employ the Voight convention. The bulk modulus B and first derivative B' can also obtained by monitoring the ratio $\frac{V}{V_0}$ of volume, V, and equilibrium volume, V_0, over a range of pressures. A numerical procedure

can then be used to fit the values of B and B' to the Birch[11] equation of state which is given by;

$$P = \frac{3}{2}B_0 \left[\left(\frac{V}{V_0}\right)^{\frac{-7}{3}} - \left(\frac{V}{V_0}\right)^{\frac{-5}{3}} \right] \left[1 + \frac{3}{4}(B' - 4) \left(\frac{V}{V_0}\right)^{\frac{-2}{3}} - 1 \right] \qquad (2.21)$$

Chapter 3

Application of the Tersoff Potential to B-C Complexies

An approach using Tersoff potentials is employed in the GULP code, to determine Bulk and Elastic properties of the $B-C$ complex materials.

3.1 B-C Crystal Structures

A possible diamond-related phase may be formed from a simple eight-atom unit cell of the diamond lattice with B or C atoms placed at various lattice points according to the nominal lattice stoichiometry[20]. Figure 3.1 shows

the B-C structures considered in the study. Supercells of various sizes can be generated from these structures as discussed later in the thesis.

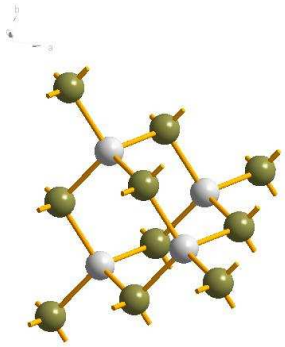

BC

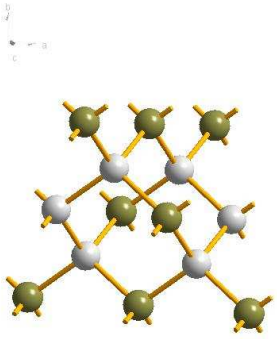

B_3C_5

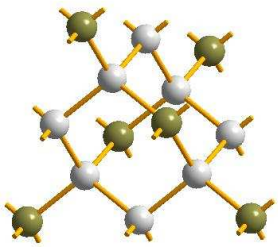

$BC_3 - a$

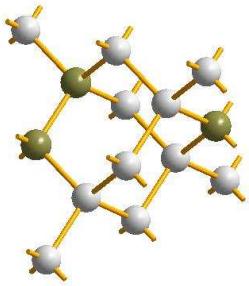

$BC_3 - b$

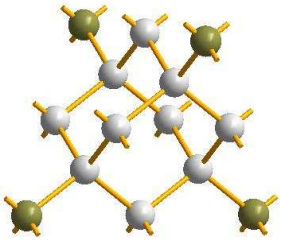

BC_7

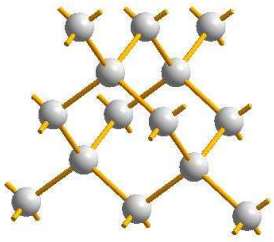

$Diamond$

Figure 3.1: B-C structures considered in this work. Dark yellow and white represent Boron and Carbon atoms, respectively.

3.2 Results

The study has been conducted for the crystalline and random phases of these structures at an absolute zero temperature (0k). The random structures are created by generating a random distribution of atoms over the crystal lattice sites then letting the geometry relax. The properties simulated are elastic constants, bulk modulus, shear modulus, Young's modulus, and total formation energies for the structures. A number of supercells were used as GULP input, namely; $1\times1\times1$(8 atoms), $4\times4\times4$(512 atoms), $5\times5\times5$(1000 atoms), and $6\times6\times6$(1728). We run MD for both the crystalline and random phases. A structural optimisation (OPT) procedure[2] was also performed to improve the quality of the starting structure prior to a dynamical simulation. The properties predicted by MD and OPT are in agreement for a smaller supercell(8-atoms) and differ as the size of the supercell increases. The OPT results is bigger for elastic constants and smaller for the total energy. Tables 3.1 to 3.4 show the predictions of MD and OPT of the total ground state energy (referred to as energy in the table), elastic constants(C_{11}, C_{12}, and C_{44}), bulk modulus (B), shear modulus (G), Young's modulus (ϵ) and the Poisson's ratio (μ).

Supercell	Compound	Energy ($eV/atom$)	$C_{11}(GPa)$	$C_{12}(GPa)$	$C_{44}(GPa)$	$B(GPa)$	$G(GPa)$	$\varepsilon(GPa)$	μ
111	BC	-7.151	598	108	344	271	304	565	0.1524
	B_3C_5	-7.202	690	112	399	305	355	658	0.1400
	BC_3(b)	-7.175	786	115	432	339	393	754	0.1285
	BC_3(a)	-7.252	825	101	456	342	417	799	0.1031
	BC_7	-7.313	932	107	545	382	492	910	0.1028
	Diamond	-7.370(-10.125)[a]	1074	102	642(576)[c]	426($433-442$)[b]	579	1056	0.0865
444	BC	-7.145	598	108	344	271	304	565	0.1524
	B_3C_5	-7.195	690	112	399	305	355	658	0.1400
	BC_3(b)	-7.174	786	115	432	339	393	754	0.1285
	BC_3(a)	-7.252	825	101	456	342	417	799	0.1031
	BC_7	-7.307	932	107	545	382	492	910	0.1028
	Diamond	-7.371(-10.125)[a]	1074	102	642(576)[c]	426($433-442$)[b]	579	1056	0.0865
555	BC	-7.145	598	108	344	271	304	565	0.1524
	B_3C_5	-7.196	690	112	399	305	355	658	0.1400
	BC_3(b)	-7.196	786	115	432	339	393	754	0.1285
	BC_3(a)	-7.252	825	101	456	342	417	799	0.1031
	BC_7	-7.308	932	107	545	382	492	910	0.1028
	Diamond	-7.370(-10.125)[a]	1074	102	642(576)[c]	426($433-442$)[b]	579	1056	0.0865
666	BC	-7.145	598	108	344	271	304	565	0.1524
	B_3C_5	-7.173	690	112	399	305	355	658	0.1400
	BC_3(b)	-7.196	786	115	432	339	393	754	0.1285
	BC_3(a)	-7.252	825	101	456	342	417	799	0.1031
	BC_7	-7.308	932	107	545	382	492	910	0.1028
	Diamond	-7.370(-10.125)[a]	1074	102	642(576)[c]	426($433-442$)[b]	579	1056	0.0865
	BC_5					($335 \pm 8GPa$)[d]			

(a) Referecce[95]

(b) Referene[96, 97]

(c) Reference[98, 99]

(d) Reference[23]

Table 3.1: Properties of crystalline phase structures predicted using OPT.

Values in brackets are experimental values.

Supercell	Compound	Energy($eV/atom$)	$C_{11}(GPa)$	$C_{12}(GPa)$	$C_{44}(GPa)$	$B(GPa)$	$G(GPa)$	$\varepsilon(GPa)$	μ
111	BC	-6.9125	538	122	255	260	236	490	0.1866
	B_3C_5	-7.202	690	113	399	305	355	658	0.1403
	BC_3(b)	-7.175	786	115	432	339	393	754	0.1284
	BC_3(a)	-7.252	825	101	456	342	417	799	0.1033
	BC_7	-7.313	932	107	546	382	492	910	0.1031
	Diamond	-7.375(−10.125)[a]	1074	102	642(576)[c]	426(433 − 442)[b]	579	1056	0.0865
444	BC	-7.07	619	129	352	292	309	574	0.1731
	B_3C_5	-7.150	692	121	403	312	352	651	0.1469
	BC_3(b)	-7.151	777	115	425	336	386	745	0.1299
	BC_3(a)	-7.227	820	102	455	343	414	792	0.103
	BC_7	-7.297	927	108	543	381	489	905	0.1042
	Diamond	-7.367(−10.125)[a]	1072	102	640(576)[c]	425(433 − 442)[b]	575	1054	0.0868
555	BC	-7.026	611	132	350	292	306	564	0.1778
	B_3C_5	-7.127	696	127	406	319	354	654	0.1526
	BC_3(b)	-7.137	776	116	422	337	384	742	0.1314
	BC_3(a)	-7.212	818	104	455	345	413	788	0.1038
	BC_7	-7.29	924	109	541	380	488	901	0.1054
	Diamond	-7.362(−10.125)[a]	1069	102	639(576)[c]	424(433 − 442)[b]	577	1052	0.0871
666	BC	-7.742	418	148	126	234	145	226	0.2094
	B_3C_5	-6.950	577	142	298	289	265	527	0.1953
	BC_3(b)	-7.172	760	121	431	335	386	734	0.1379
	BC_3(a)	-7.172	766	119	430	335	387	734	0.1338
	BC_7	-7.289	919	110	537	380	484	894	0.1071
	Diamond	-7.370(−10.125)[a]	1074	102	642(576)[c]	426(433 − 442)[b]	579	1056	0.08651

(a) Refererecce[95]

(b) Referene[96, 97]

(c) Reference[98, 99]

Table 3.2: Properties of crystalline phase structures predicted using MD. Values in brackets are experimental values

Supercell	Compound	Energy ($eV/atom$)	$C_{11}(GPa)$	$C_{12}(GPa)$	$C_{44}(GPa)$	$B(GPa)$	$G(GPa)$	$\varepsilon(GPa)$	μ
111	BC	-6.9125	541	123	256.4	262	238	493	0.186
	B_3C_5	-7.0375	595	127	370	298	308	642	0.1904
	BC_3(b)	-7.175	785	115.5	432	339	393	753	0.1294
	BC_3(a)	-7.252	759	116	483	342	417	799	0.1371
	BC_7	-7.313	932	107	546	382	492	910	0.1031
	Diamond	-7.362(-10.125)[a]	1074	102	642(576)[c]	426($433-442$)[b]	579	1056	0.08653
444	BC	-6.779	458	151	158	247	163	344	0.2436
	B_3C_5	-6.994	606	136	309	290	280	541	0.1843
	BC_3(b)	-7.149	758	123	418	333	377	712	0.1391
	BC_3(a)	-7.164	761	122	430	334	385	721	0.1388
	BC_7	-7.277	916	111	533	378	481	886	0.108
	Diamond	-7.367(-10.125)[a]	1072	102	640(576)[c]	425($433-442$)[b]	578	1054	0.0868
555	BC	-6.756	430	156	179	247	162	351	0.2698
	B_3C_5	-6.961	589	137	304	287	272	541	0.1878
	BC_3(b)	-7.14	723	124	422	333	378	712	0.1404
	BC_3(a)	-7.128	750	123	416	331	374	711	0.1402
	BC_7	-7.266	906	112	528	377	476	884	0.1099
	Diamond	-7.362(-10.125)[a]	1069	102	639(576)[c]	424($433-442$)[b]	577	1052	0.0871
666	BC	-6.7419	418	148	126	234	145	226	0.2093
	B_3C_5	-6.946	577	142	298	289	265	527	0.1953
	BC_3(b)	-7.120	744	128	419	335	374	715	0.147
	BC_3(a)	-7.122	746	125	417	333	375	713	0.1426
	BC_7	-7.250	905	113	529	377	476	880	0.1108
	Diamond	-7.358(-10.125)[a]	1067	102	638(576)[c]	424($433-442$)[b]	575	1049	0.08741

(a) Refererecce[95]

(b) Referene[96, 97]

(c) Reference[98, 99]

Table 3.3: Properties of the random phase structures predicted using MD.

Values in brackets are experimental values

Supercell	Compound	Energy ($eV/atom$)	$C_{11}(GPa)$	$C_{12}(GPa)$	$C_{44}(GPa)$	$B(GPa)$	$G(GPa)$	$\varepsilon(GPa)$	μ
111	BC	-6.916	542	122	258	262	238	494	0.185
	B_3C_5	-7.043	596	126	370	298	309	643	0.189
	BC_3(b)	-7.175	785	115	432	338	393	754	0.1287
	BC_3(a)	-7.252	759	116	483	342	417	799	0.1372
	BC_7	-7.309	932	107	545	382	492	910	0.1028
	Diamond	-7.370$(-10.125)^a$	1074	102	642(576)^c	426(433 − 442)^b	579	1056	0.08651
444	BC	-6.836	479	143	202	250	192	380	0.2331
	B_3C_5	-7.027	618	132	320	292	289	559	0.1775
	BC_3(b)	-7.170	767	120	426	335	384	725	0.1353
	BC_3(a)	-7.186	769	120	435	336	391	733	0.1357
	BC_7	-7.287	921	110	536	380	483	893	0.1072
	Diamond	-7.371$(-10.125)^a$	1074	102	642 (576)^c	426 (433 − 442)^b	579	1056	0.08651
555	BC	-6.830	469	144	211	254	191	410	0.2339
	B_3C_5	-7.009	608	132	316	291	284	567	0.1791
	BC_3(b)	-7.175	766	120	431	335	387	729	0.1346
	BC_3(a)	-7.159	763	120	425	334	383	728	0.1355
	BC_7	-7.284	915	111	534	379	481	894	0.1082
	Diamond	-7.371$(-10.125)^a$	1074	102	642(576)^c	426(433 − 442)^b	579	1056	0.08651
666	BC	-6.836	459	143	214	249	192	400	0.2407
	B_3C_5	-7.021	609	132	320	291	287	567	0.1785
	BC_3(b)	-7.172	760	121	431	335	386	734	0.1379
	BC_3(a)	-7.172	766	119	430	335	387	734	0.1338
	BC_7	-7.289	919	110	537	380	484	894	0.1071
	Diamond	-7.370$(-10.125)^a$	1074	102	642(576)^c	426(433 − 442)^b	579	1056	0.08651

(a) Refererece[95]

(b) Referene[96, 97]

(c) Reference[98, 99]

Table 3.4: Properties of the random phase structures predicted using OPT.

Values in brackets are experimental values.

We note the difference in the calculated values from experimental results in diamond for the total ground state energy and C_{44}, but there is agreement for B.

Cell parameters

Cell parameters (a, b, and c) and cell angles (α, β, and γ) for all structures are examined. A conventional cell parameter average ($\tilde{a}$) is also calculated, using equation 3.1;

$$\tilde{a} = \frac{a + b + c}{3} \tag{3.1}$$

Taking the average here is justified since the structures are almost cubic, as can be seen from table 3.5.

Crystal MD	a(Å)	b(Å)	c(Å)	ã(Å)	α°	β°	γ°
BC	3.648	3.648	3.6485	3.648	90	90	90
B_3C_5	3.635	3.6346	3.635	3.635	90	90	90
BC_3(b)	3.601	3.601	3.601	3.601	89.69	89.69	90.32
BC_3(a)	3.603	3.603	3.620	3.609	90	90	90
BC_7	3.586	3.586	3.586	3.586	90	90	90
Diamond	3.566	3.566	3.566	3.566(3.567)[a]	90	90	90
Crystal OPT							
BC	3.662	3.662	3.662	3.662	90	90	90
B_3C_5	3.634	3.634	3.634	3.634	90	90	90
BC_3(b)	3.602	3.602	3.602	3.602	89.68	89.68	90
BC_3(a)	3.603	3.603	3.620	3.609	90	90	90
BC_7	3.586	3.586	3.586	3.586	90	90	90
Diamond	3.5656	3.5656	3.5656	3.5656(3.567)[a]	90	90	90
Random MD							
BC	3.648	3.648	3.649	3.648333333	89	89	89
B_3C_5	3.641	3.615	3.615	3.624	89.2	90	90
BC_3(b)	3.601	3.603	3.602	3.602	89.7	90.3	89.7
BC_3(a)	3.620	3.603	3.603	3.609	90	90	90
BC_7	3.586	3.586	3.586	3.586	90	90	90
hline Diamond	3.566	3.566	3.566	3.566(3.567)[a]	90	90	90
Random OPT							
BC	3.648	3.648	3.648	3.648	89	89	89
B_3C_5	3.643	3.614	3.614	3.624	89.2	90	90
BC_3(b)	3.602	3.602	3.602	3.602	89.7	90.3	89.7
BC_3(a)	3.620	3.603	3.603	3.608666667	90	90	90
BC_7	3.586	3.586	3.586	3.586	90	90	90
Diamond	3.566	3.566	3.566	3.566(3.567)[a]	90	90	90
BC_5	(3.635 ± 0.006)[d]						

(a) Refererece[95]

(d) Reference[100]

Table 3.5: Cell parameters predicted for the B-C structures. Values in brackets are experimental values

3.2.1 Graphical representation of the results for the B-C crystal structures

A graphical analysis of some properties predicted in this work is performed to examine the various trends described below. Plots of the number of each type of bonds (B-C, C-C, and B-B bonds) against the B-C trend are done as shown in figure 3.2. Figures 3.3 to 3.4 show the total energy dependence on the trend while the graphs in figure 3.5 to 3.6 show the dependence on the B-C trend of the elastic parameters, B, G, and ϵ.

The variation of the elastic constants with the B-C trend is graphically represented in figure 3.7 to 3.8, while the calculated cell constants are also plotted against the trend as shown in figure 3.9.

For the Random Phases it is important that the size of the supercell chosen for the randomization process does not affect the final result. To confirm this is the case, various sizes of the supercell were tested to ensure convergence and the value of the moduli are as shown in figure 3.10, where the numbers 0, 1, 2 and 3 on the horizontal axis represent systems containing 8, 512, 1000, and 1728 atoms, respectively. It should be noted that in figure 3.10 BC_3

refers to $BC_3 - b$ because it is the lower energy of the two BC_3 structures.

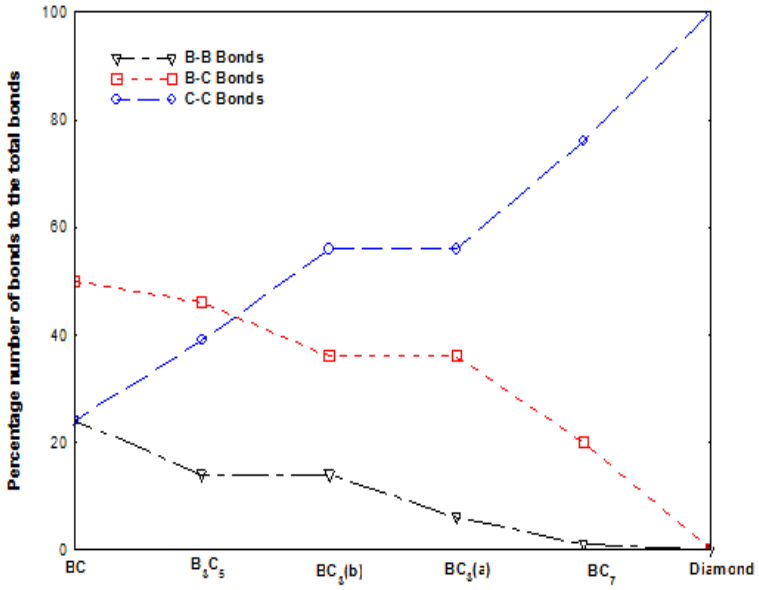

Figure 3.2: Percentage of the number of bonds versus the composition for a random phase

Energy difference and ratio of lattice constants

The difference in energy ($\triangle E$) between the random structures and their crystalline countepart is also explored, Where;

$$\triangle E = E_{crystal} - E_{random} \tag{3.2}$$

$$E_{crystal} = energy\, per\, atom\, for\, the\, crystalline\, phase \tag{3.3}$$

$$E_{random} = energy\, per\, atom\, for\, the\, random\, phase \tag{3.4}$$

Figure 3.11 shows the trend in $\triangle E$ as the number carbon-carbon bonds increases. The effect of the random distribution of boron and carbon on the lattice constants is studied. This is done by taking the ratio of the cell parameters for each phase (i.e $\frac{\tilde{a}_{random}}{\tilde{a}_{crystal}}$) and is shown in figure 3.12. The ground state energy is seen to be decreasing with the concentration and so are the elastic constants and the Poisson ratio. Values of the cell constants are decreasing with the concentration.

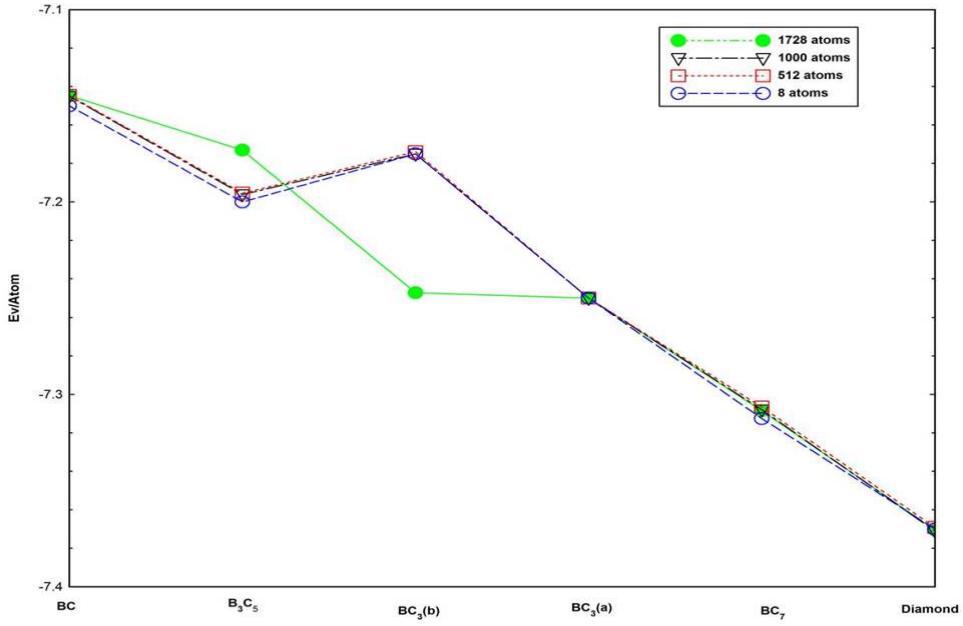

(a)

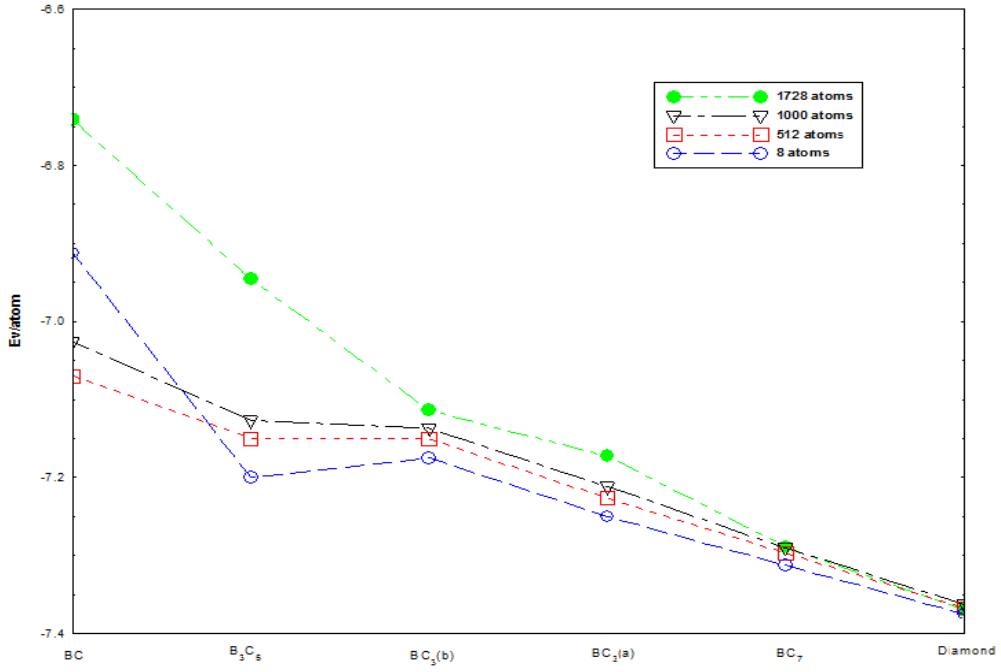

(a)

Figure 3.3: Energy for crystal structures. (a) is for OPT, while (b) is for MD. The horizontal axes are showing the composition

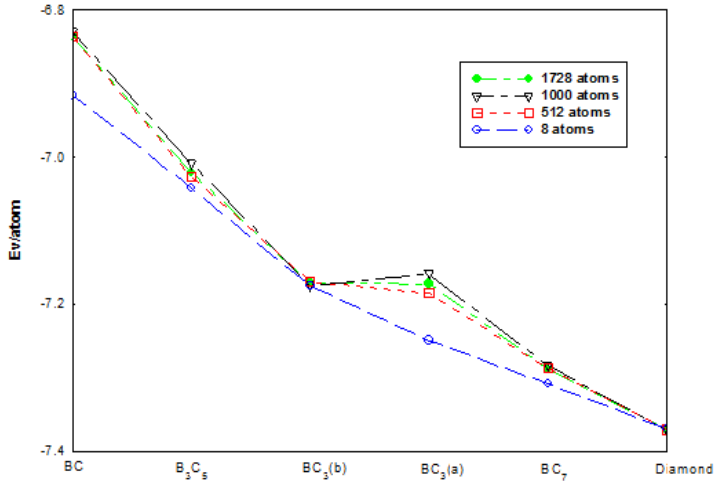

(a)

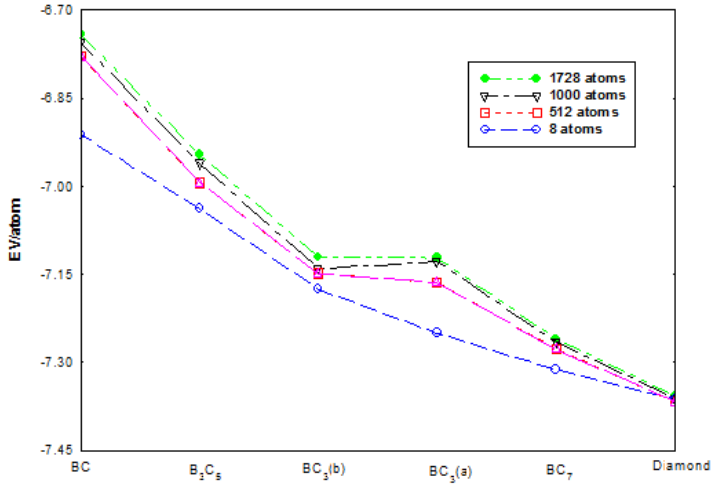

(b)

Figure 3.4: Energy for random structures. (a) is for OPT, while (b) is for MD. The horizontal axes are showing the composition

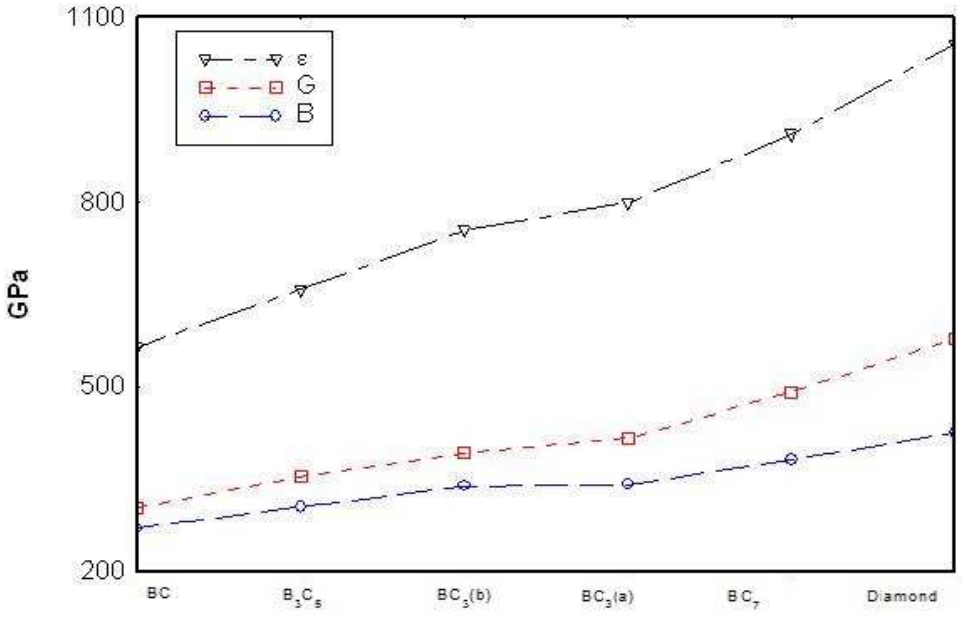

(a)

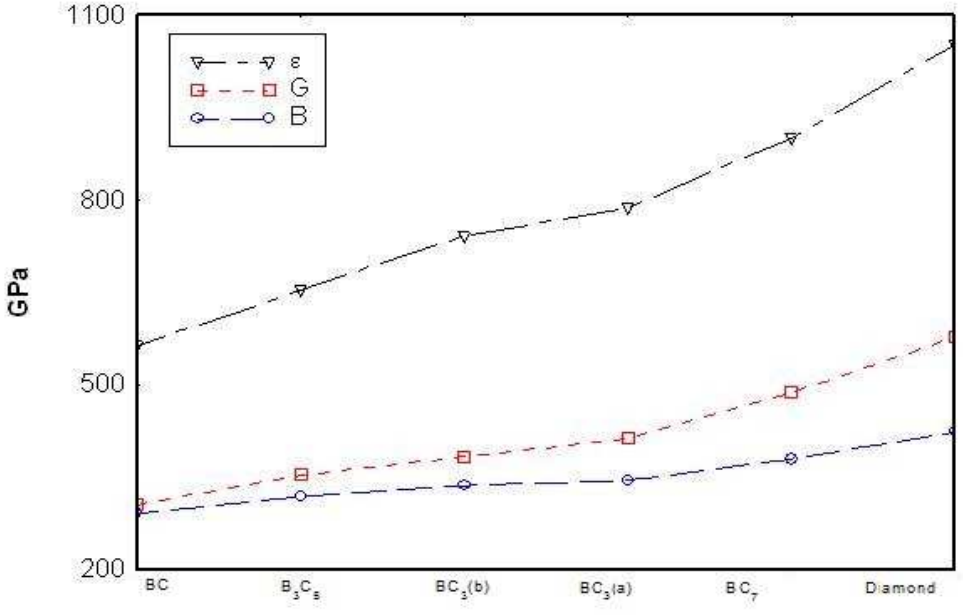

(b)

Figure 3.5: B, G, and ϵ for crystal structures. (a) is for OPT, while (b) is for MD. The horizontal axes are showing the composition

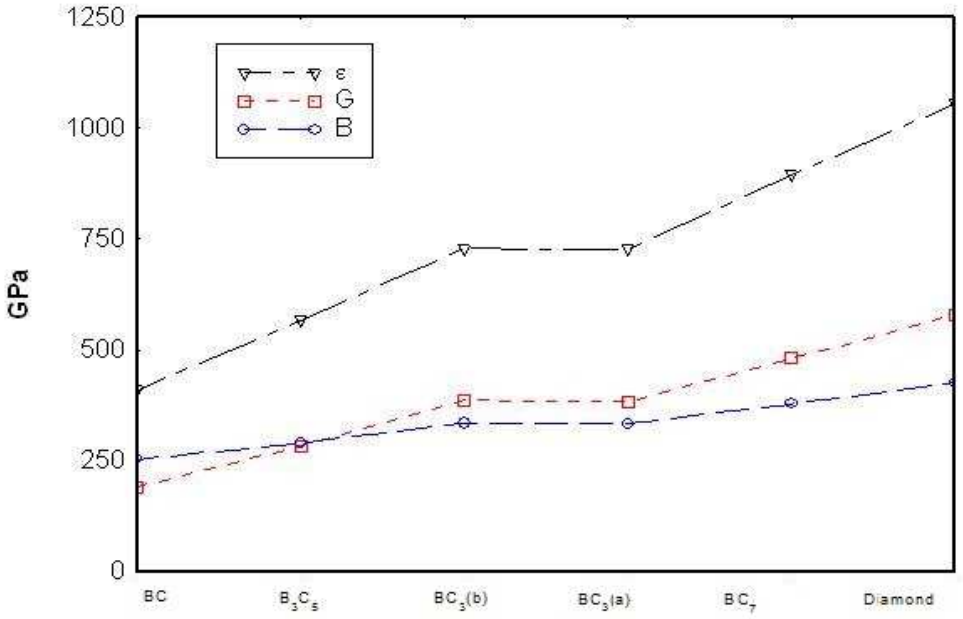

(a)

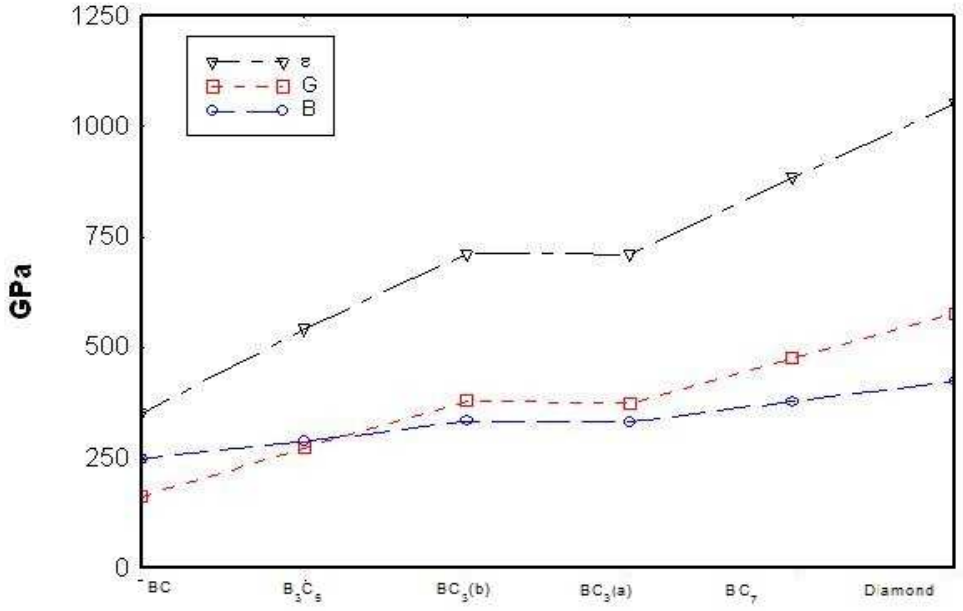

(b)

Figure 3.6: B, G, and ϵ for random structures. (a) is for OPT, while (b) is for MD. The horizontal axes are showing the composition

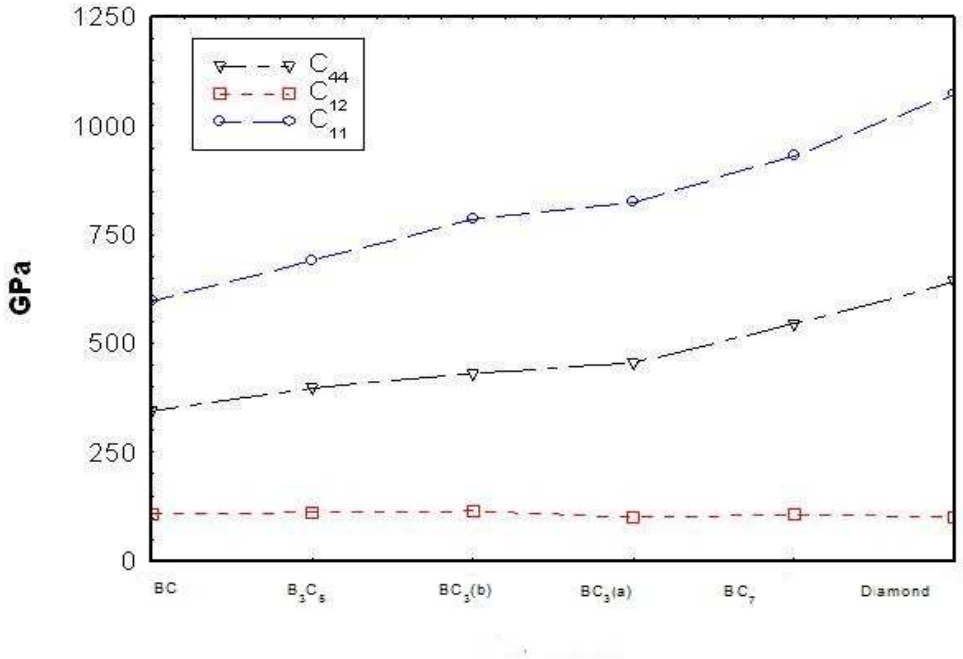

(a)

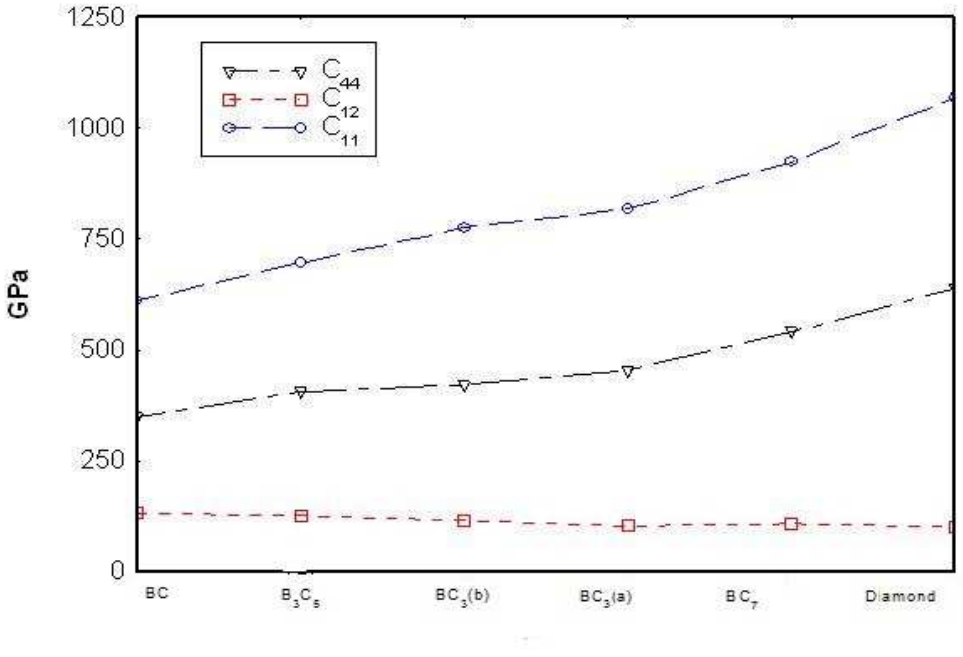

(b)

Figure 3.7: Elastic constants for crystal structures. (a) is for OPT, while (b) is for MD. The horizontal axes are showing the composition

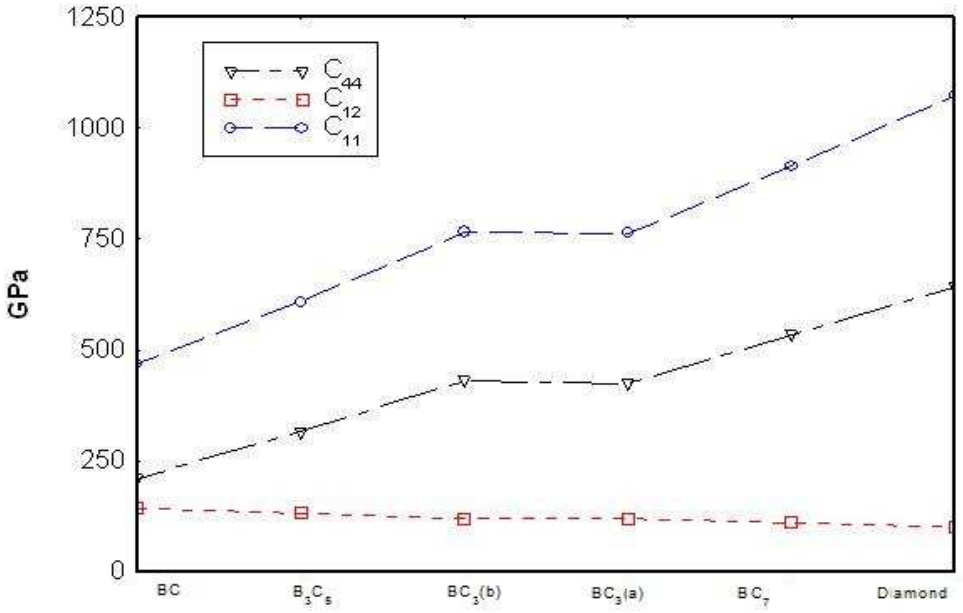

(a)

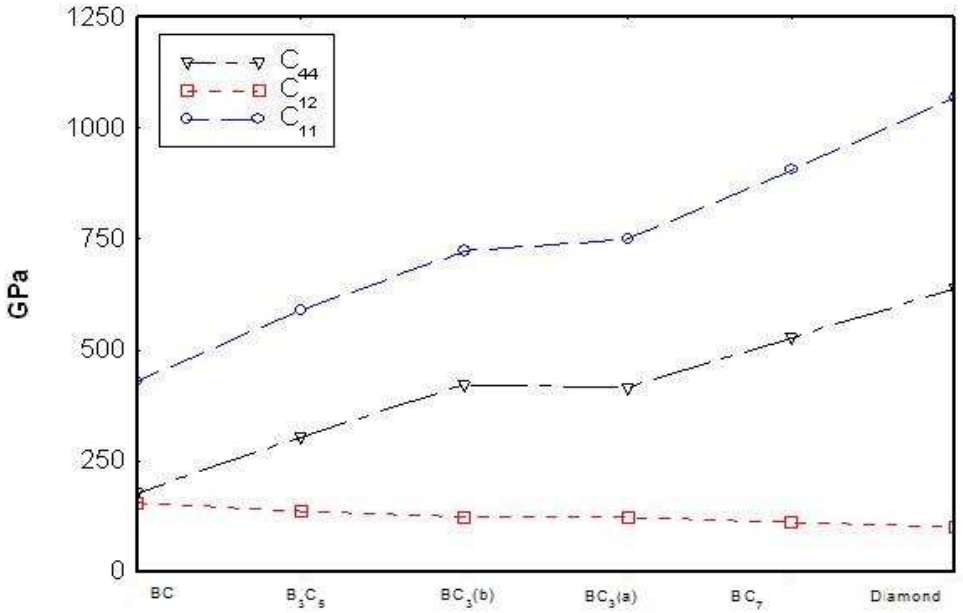

(b)

Figure 3.8: Elastic constants for the random structures. (a) is for OPT, while (b) is for MD. The horizontal axes are showing the composition

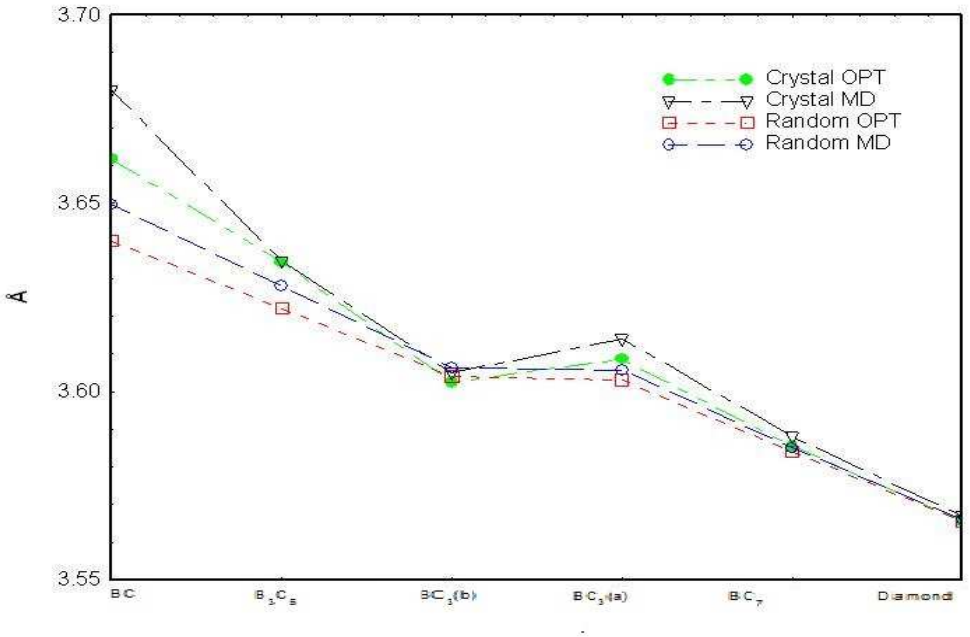

Figure 3.9: Cell constant against Composition

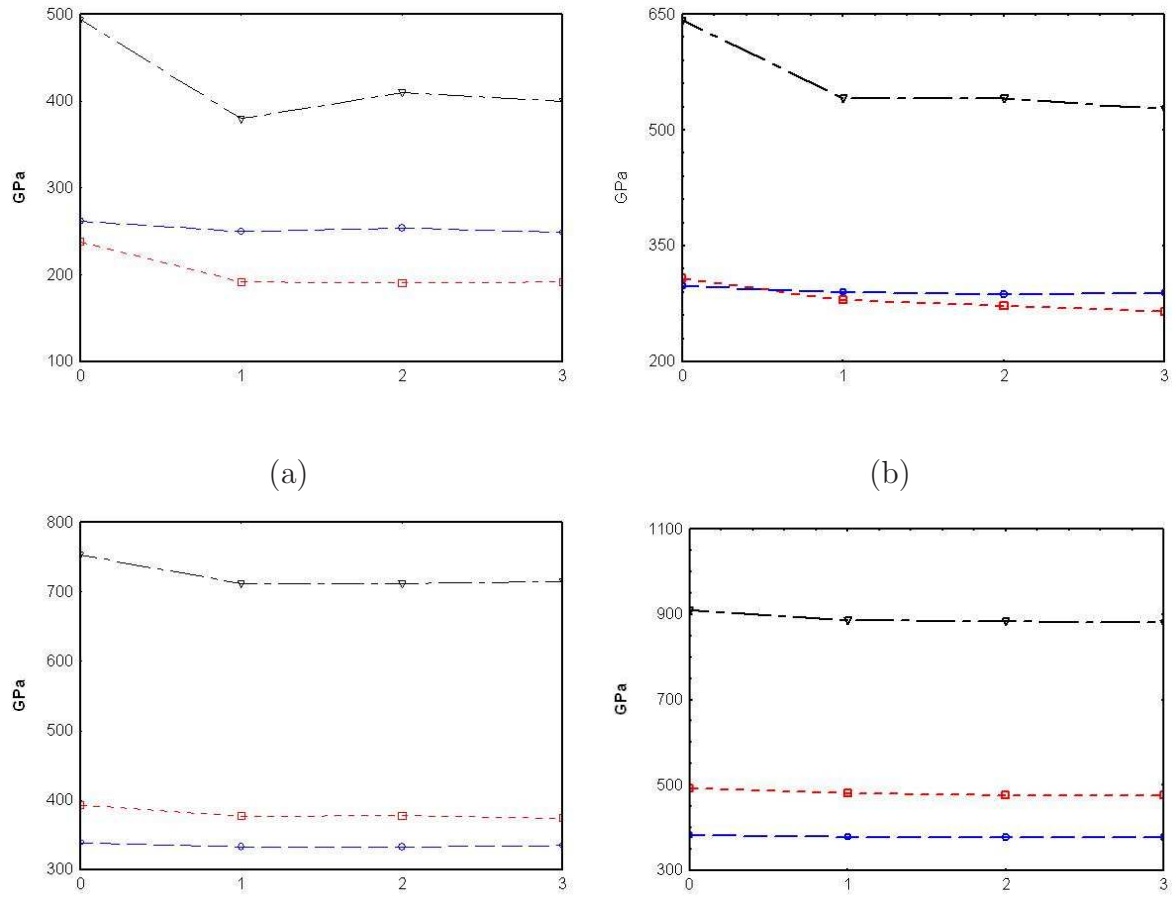

Figure 3.10: Bulk(◯), shear(⊟) and Young(▽) moduli for various sizes of the supercells with random B and C distribution. (a), (b), (c) and (d) represents BC, B_3C_5, BC_3 and BC_7, respectively. The horizontal axes are showing the composition

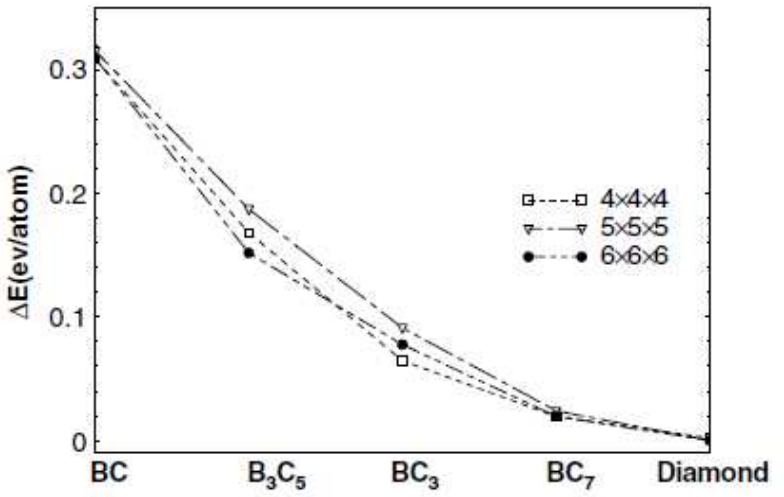

Figure 3.11: Energy difference of the crystal and random phase against B-C trend

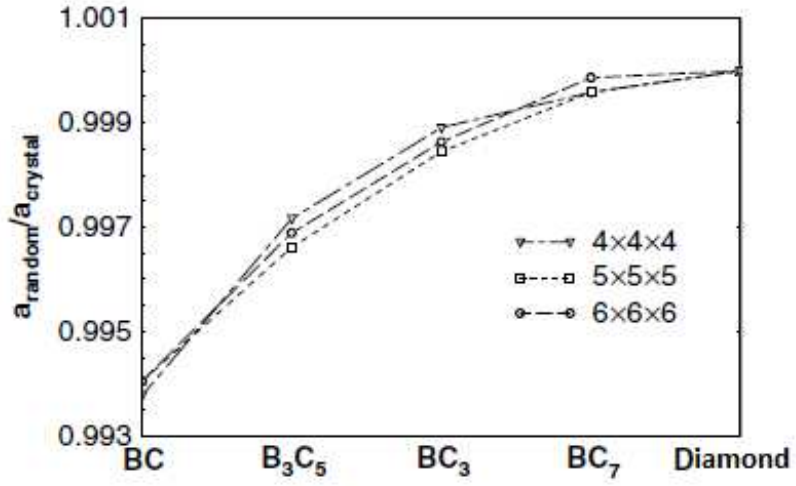

Figure 3.12: Ratio of the random and crystal lattice cell constants

Chapter 4

Tersoff Potential Application to B-C-N Complexes

Using the Gulp code, the Tersoff potentials were applied to study the trends of the B-C-N complexies as highlighted in Chapter 1. Each trend consist of 5 structures. The trends are are in relation to the composition of B, C and N in the structures and they are; BC to BN, BN to C, and C to BC. The trend $B_{4-x}C_{4+x}$, $(x = 0 \ldots 4.)$ is as outlined in the previous chapter. Only $BC_3 - b$ is considered for the BC_3 structure since it is of lower energy. Figure 4.1 shows the structures of the trend$B_4N_{4-x}C_x$, $(x = 0 \ldots 4.)$, while figure 4.2 shows the structures of the trend $B_{4-x}N_{4-x}C_{2x}$, $(x = 0 \ldots 4.)$. BN and

Diamond have been shown previously and are thus omitted here.

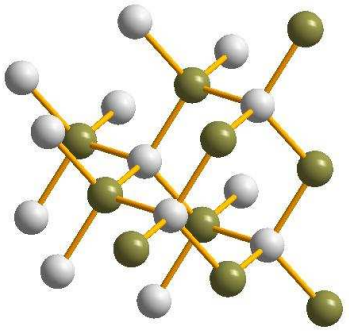

BC

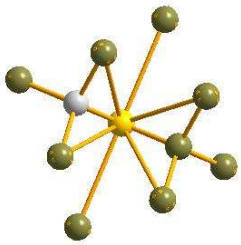

B_4C_3N

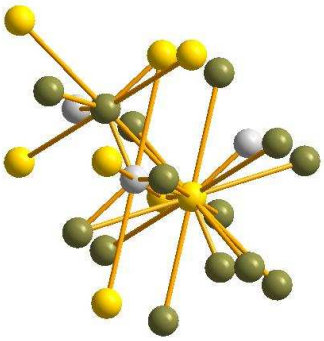

B_2CN

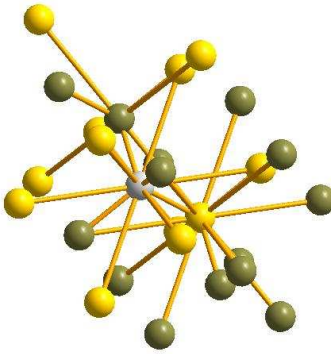

B_4CN_3

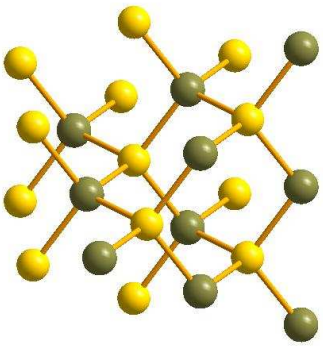

BN

Figure 4.1: B-C-N structures considered for the composition $B_4N_{4-x}C_x$, ($x = 0 \ldots 4.$) , dark yellow, white and yellow represent Boron, Carbon and Nitrogen atoms, respectively.

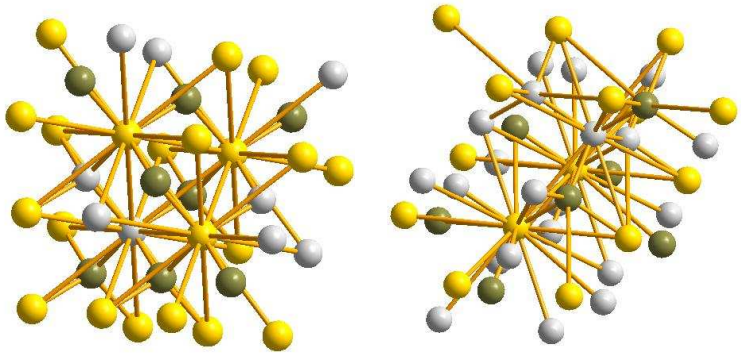

$B_3C_2N_3$ BC_2N

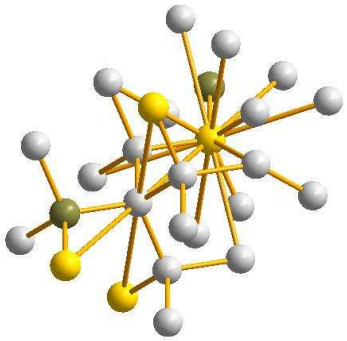

BC_6N

Figure 4.2: B-C-N structures considered for the composition $B_{4-x}N_{4-x}C_{2x}$, $(x = 0 \ldots 4.)$, dark yellow, white and yellow represent Boron, Carbon and Nitrogen atoms, respectively.

4.1 Comparison of the predictions of the Two sets of Tersoff Potential Parameters for Nitrogen

Since there are two sets of Tersoff parameters for Nitrogen as tabulated in Table2.1,The quality of the predictions of the two sets is first looked into. Considering a 512 atoms supercell, we employ the two diffent Tersoff potentials, for the simulation of the structures, using only OPT. Tables 4.1 and 4.2 show the results for the total ground state formation energy, C_{11}, C_{12}, C_{44}, Bulk modulus (B), Shear modulus (G), Young's modulus (ϵ), and the Poisson ratio (ν) using parameters Set 1. This was also done for Set 2 and the results are tabulated in Tables 4.3 and 4.4.

Structure	Energy (Ev/atom)	C_{11} (GPa)	C_{12} (GPa)	C_{44} (GPa)	B (GPa)	G (GPa)	ε (GPa)	μ
BC	-7.14	598	108	344	271	304	565	0.152
B_4C_3N	-7.02	560	164	288	296	252	485	0.23
B_2CN	-6.89	541	230	260	322	207	403	0.33
B_4CN_3	-6.77	506	273	205	351	169	314	0.35
BN	-6.65	494 (820)[a]	331 (190)[a]	176 (480)[a]	386 (400)[a]	138	228	0.40
$B_3C_2N_3$	-7.04	1662	755	959	1056	752	846	0.28
BC_2N	-7.38	955	61.4	1152 (355)[a],(282)[b]	817.5	656	946.4	
BC_6N	-7.10	979	169	531.2	439	480	924	0.15
$Diamond(C_8)$	-7.37	1074	102	641	426	579	1056	0.087
BC_7	-7.31	932	107	545	382	492	910	0.103
BC_3	-7.25	825	101	456	342	417	799	0.103
B_3C_5	-7.20	690	112	399	305	355	658	0.140
BC	-7.14	598	108	344	271	304	565	0.152

(a) Refererece[101]

(b) Refererece[55]

Table 4.1: Predicted properties of crystal phase using Parameter Set 1 of B-C-N. Values in brackets are experimental values. Energy here refers to the ground state total formation energy

Structure	Energy (Ev/atom)	C_{11} (GPa)	C_{12} (GPa)	C_{44} (GPa)	B (GPa)	G (GPa)	ε (GPa)	μ
BC	-6.84	466	139	220	249	197	408	0.23
B_4C_3N	-6.96	342	152	235	261	184	332	0.281
B_2CN	-7.20	508	235	248	346	211	374	0.31
B_4CN_3	-7.26	657	227	325	395	261	562	0.26
BN	-6.95	380	217	140	399	121	201	0.364
$B_3C_2N_3$	-7.20	695	329	362	485	304	549	0.29
BC_2N	-7.41	818	242	470	445	393	670	0.24
BC_6N	-7.25	970	210	552	449	492	900	0.16
$Diamond(C_8)$	-7.37	1074	102	642	426	579	1057	0.086
BC_7	-7.29	918	110	537	380	483	900	0.107
BC_3	-7.21	781	117	440	338	397	746	0.13
B_3C_5	-7.02	627	121	308	291	289	573	0.17
BC	-6.84	466	139	220	250	197	408	0.23

Table 4.2: Predicted properties of random phase using Parameter Set 1 of B-C-N. Energy here refers to the ground state total formation energy

Structure	Energy (Ev/atom)	C_{11} (GPa)	C_{12} (GPa)	C_{44} (GPa)	B (GPa)	G (GPa)	ε (GPa)	μ
BC	-7.15	598	108	344	271	304	565	0.15
B_4C_3N	-6.84	663	101	380	288	341	636.88	0.132
B_2CN	-6.53	721	94	431	307	382	715	0.11
B_4CN_3	-6.23	813	83	471.1	327	429	798	0.092
BN	-5.92	896	73.2	526	347	480	885	0.076
$B_3C_2N_3$	-6.20	911	93.6	534	366	484	894	0.093
BC_2N	-6.53	939	82.9	555	379	497	934	0.097
BC_6N	-6.93	989	101	580	397	526	970	0.092
$Diamond(C_8)$	-7.37	1074	102	642	426	579	1057	0.087
BC_7	-7.31	932	107	545	382	492	910	0.103
BC_3	-7.25	825	101	456	342	417	799	0.103
B_3C_5	-7.20	690	112	399	305	355	659	0.140
BC	-7.14	598	108	344	271	304	565	0.152

Table 4.3: Predicted properties of crystal phase using Parameter Set 2 of B-C-N. Energy here refers to the ground state total formation energy

Structure	Energy (Ev/atom)	C_{11} (GPa)	C_{12} (GPa)	C_{44} (GPa)	B (GPa)	G (GPa)	ε (GPa)	μ
BC	-6.76	448	148	219	250	189	384	0.241
B_4C_3N	-6.43	525	137	222	266	215	466	0.21
B_2CN	-6.14	535	135	360	290	268	622	0.169
B_4CN_3	-5.89	745	107	348	319	336	719	0.125
BN	-5.85	896	73	526	347	480	885	0.076
$B_3C_2N_3$	-6.012	859	106	452	356	423	834	0.106
BC_2N	-6.22	846	114	517	366	449	875	0.109
BC_6N	-6.88	970	102	569	393	515	953	0.095
$Diamond(C_8)$	-7.35	1074	102	642	426	579	1056	0.0865
BC_7	-7.25	915	111	537	380	484	893	0.108
BC_3	-7.12	759	125	432	335	386	723	0.137
B_3C_5	-6.95	602	137	319	291	284	543	0.181
BC	-6.76	448	148	219	250	189	384	0.241

Table 4.4: Predicted properties of random phase using Parameter Set 2 of B-C-N. Energy here refers to the ground state total formation energy

The Moduli values from the four different structural types simulated are plotted against the B-C-N composition, as shown in Table 4.5. The percentage of number bonds are also examined into. The plotted graphs are as shown in figures 4.3 and 4.4.

Trend	structure	C-C	B-N	C-N	N-N	B-B	B-C
BC to BN	BC	30	0	0	0	30	40
	B_4C_3N	16	10	8	0	33	33
	B_2CN	5	23	12	5	34	22
	B_4CN_3	0	33	11	10	33	13
BN to C	BN	0	50	0	25	25	0
	$B_3C_2N_3$	5	27	17	17	17	17
	BC_2N	36	11	22	6	6	22
	BC_6N	70	2	14	0	0	14
C to BC	$Diamond$	100	0	0	0	0	0
	BC_7	86	0	0	0	1	12
	BC_3	69	0	0	0	4	27
	B_3C_5	49	0	0	0	14	37
	BC	25	0	0	0	25	50

Table 4.5: Table showing the B-C-N structures's number of bonds as a percentage of the total number of bonds of a structure

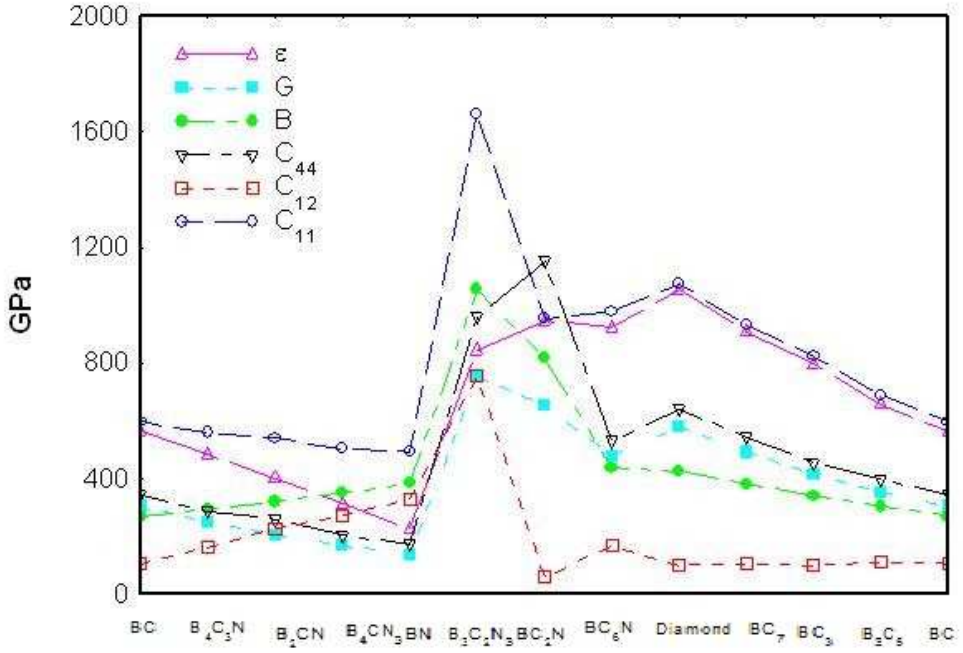

(a)

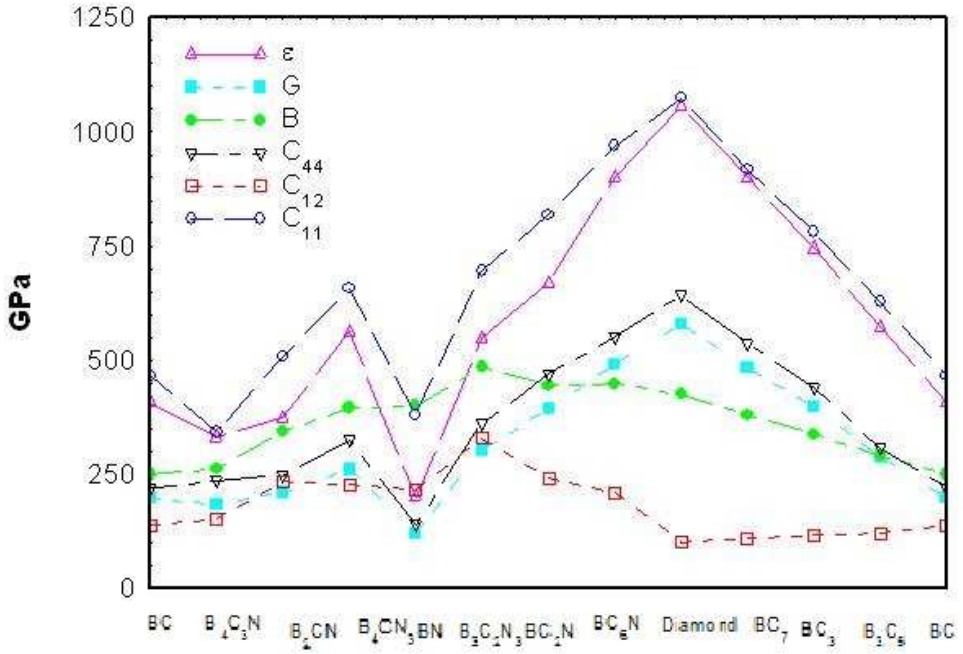

(b)

Figure 4.3: Bulk Moduli and elastic constants in units of GPa as shown on the vertical axes, with Set 1 parameters. (a) and (b) represent the crystal and random phase, respectively. The horizontal axes represent the composition of the structures

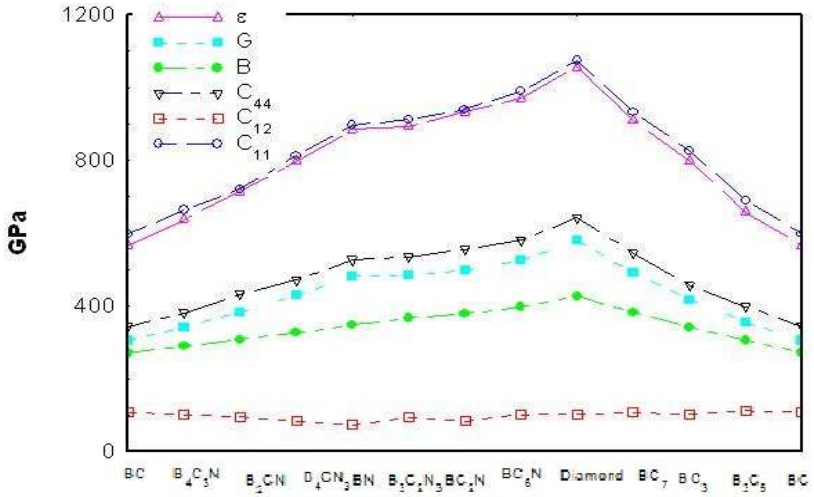

(a)

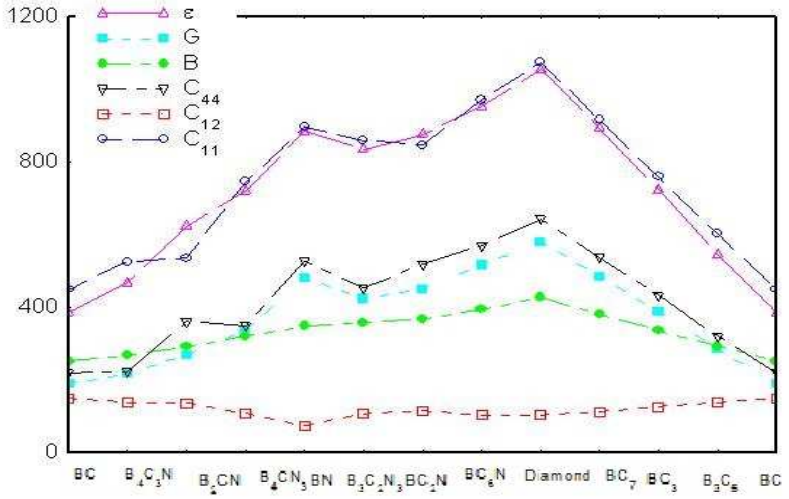

(b)

Figure 4.4: Bulk Moduli and elastic constants in units of GPa as shown on the vertical axes, with Set 2. (a) and (b) represent the crystal and random phase, respectively. The horizontal axes represent the composition of the structures

4.2 Further Results for B-C-N with Parameter Set 2

Parameter Set 2 for nitrogen appears to be yield better results than Parameter Set 1. This work is extended by only considering the Set 2 parameters.Set 1 parameters is unphysical as seen in comparing figure 4.3 with figure 4.4 compared with Set . the work was then furthered by only considering Parameter Set 2. The supercell size (number of atoms) is varied in the GULP input.

4.2.1 Crystalline Phases results

The $1 \times 1 \times 1$ (8 atoms) is considered for the crystal phase. Tables 4.6 and 4.7 shows properties obtained. Two approaches are used for calculating the cell constants. The first is to find the average of the 3 cell constants, as done in the previous chapter, shown in equation 4.1.In the other approach, the square root of the total volume, V, per atom, shown in equation 4.2. A dependance of these properties on the B-C-N trend is clearly depicted in the figures 4.5 to 4.6. We note that the Total formation energy per atom is maximum at BN and minimum at diamond. the plot of the cell constants against the composition is showing an almost parabolic curve, with a turning

Structure	a_1(Å)	a_2(Å)	α^0	β^0	γ^0
BC	3.662	3.662	90	90	90
B_4C_3N	3.651	3.651	90	90	90
B_2CN	3.64	3.64	90	90	90
B_4CN_3	3.63	3.63	90	90	90
BN	3.62(3.617)[a]	3.62(3.617)[a]	90	90	90
$B_3C_2N_3$	3.59	3.59	89.76	90.24	90.24
BC_2N	3.58(3.602)[a], (3.64)[b]	3.58(3.602)[a], (3.64)[b]	90	90	90
BC_6N	3.568	3.567	90.3	90.3	89.7
$Diamond(C_8)$	3.566	3.565	90	90	90
BC_7	3.586	3.585	90	90	90
BC_3	3.608	3.609	90	90	90
B_3C_5	3.634	3.634	90	90	90
BC	3.662	3.662	90	90	90

(a) Reference[101]

(b) Reference[55]

Table 4.6: Table of properties of crystal phase of B-C-N structures, Values in brackets are experimental values

point minimum at Diamond.

$$a_1 = \frac{a+b+c}{3} \tag{4.1}$$

$$a_2 = \sqrt{V} \tag{4.2}$$

Structure	Energy(eV/atom)	C_{11}	C_{12}	C_{44}	B	G	ε	μ
BC	-7.14	598	108	344	271	304	565	0.152
B_4C_3N	-6.84	663	101	380	288	341	637	0.13
B_2CN	-6.54	721	94	431	307	382	722	0.112
B_4CN_3	-6.23	813	83.3	471	327	429	798	0.929
BN	-5.9	896 (820)[a]	73 (190)[a]	526 (480)[a]	347 (400)[a]	480 (409)[c]	885 (973)[c]	0.076
$B_3C_2N_3$	-6.2	911	93.7	535	366	484	894	0.0932
BC_2N	-6.538	940	83	555 (355)[a], (282)[b]	379	497	934	0.0965
BC_6N	-6.925	989	101	580	397	526	970	0.0924
$Diamond(C_8)$	-7.37	1074	102	642	426	579	1056	0.08651
BC_7	-7.309	932	107	545	382	492	910	0.103
BC_3	-7.25	825	101	456	342	417	799	0.122
B_3C_5	-7.196	690	112	399	305	355	658	0.14
BC	-7.144	598	108	344	271	304	565	0.152

(a) Reference[101]

(b) Reference[55]

(c) Reference[18]

Table 4.7: Cell properties of crystal phase of B-C-N structures. The Elastic properties are expresse in units of GPa. Energy refers to the total formation energy. Values in brackets are experimental values

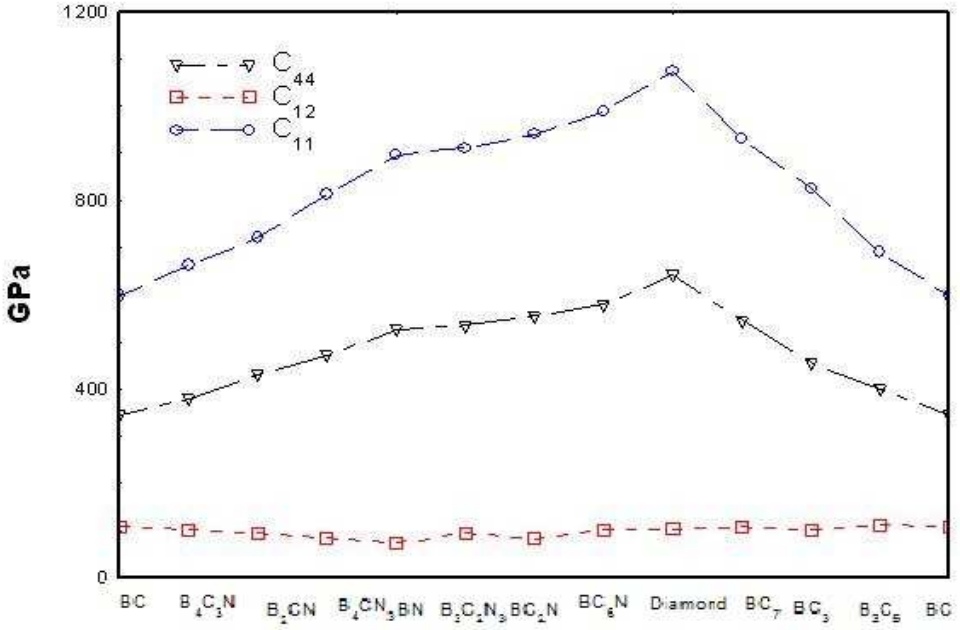

(a)

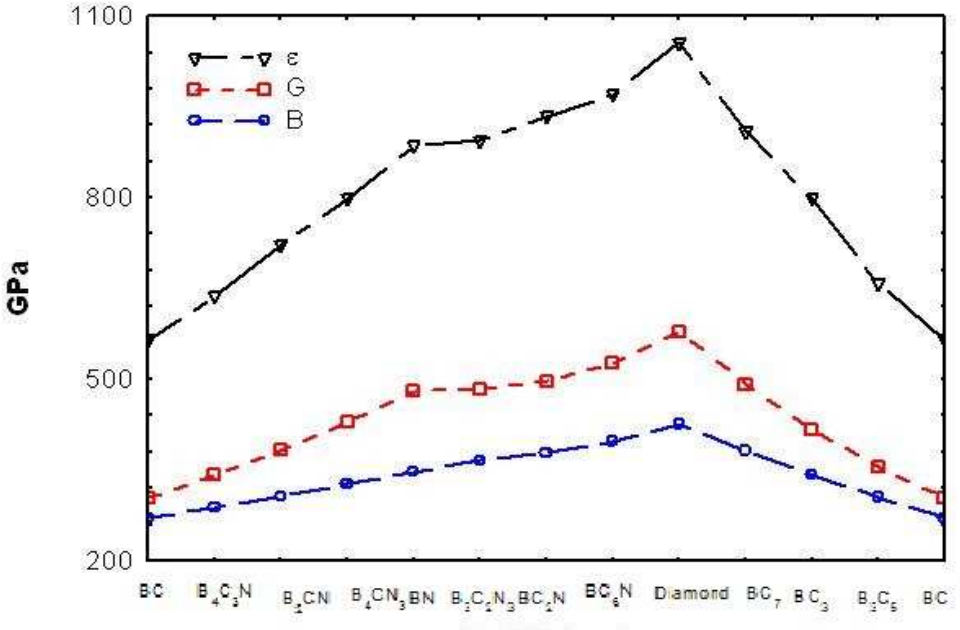

(b)

Figure 4.5: (a) Elastic constants, and (b) Moduli for the crystal phase structures. The horizontal axes represent the trend in the B-C-N composition

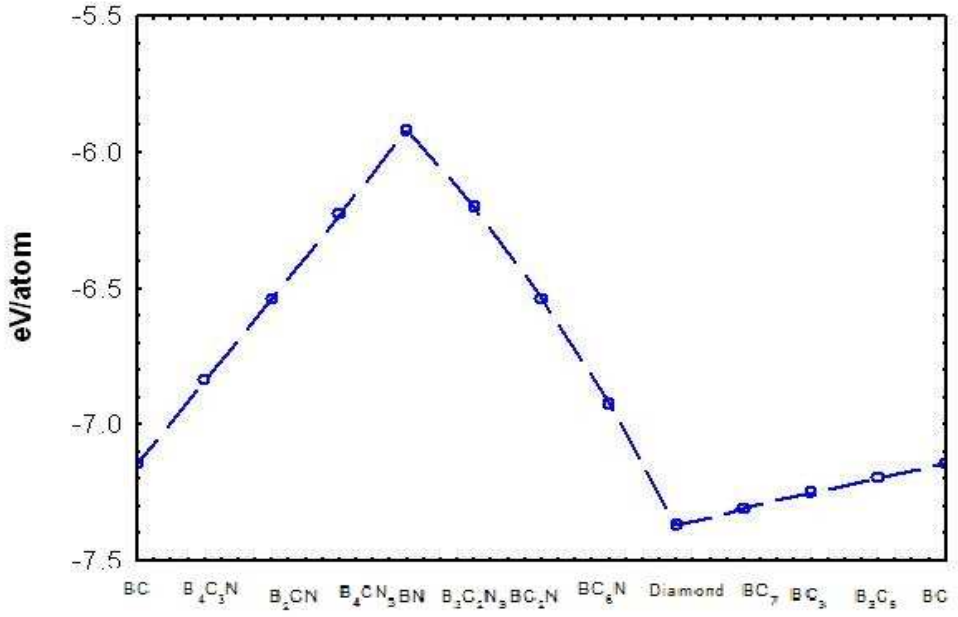

(a)

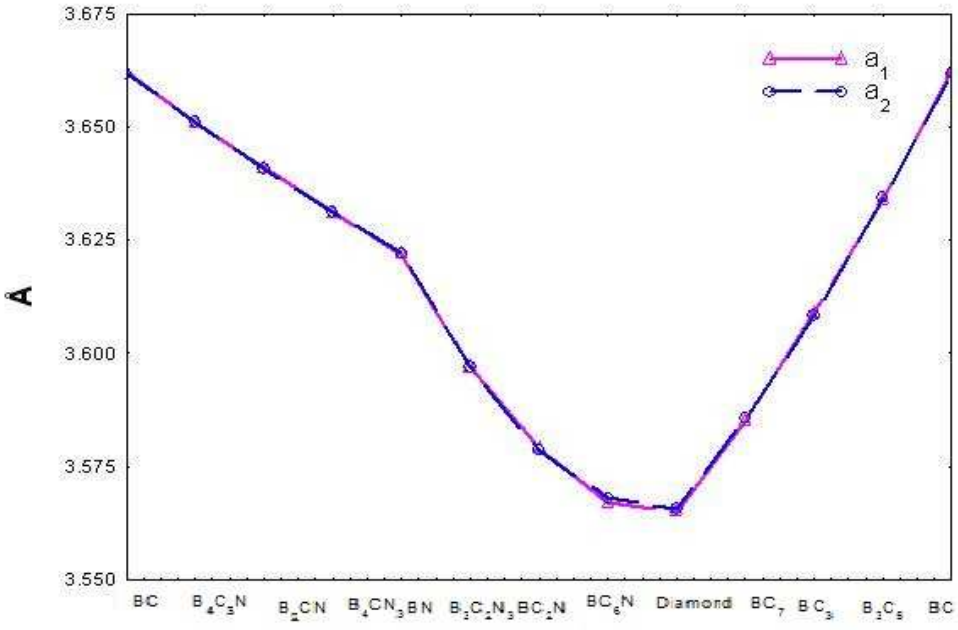

(b)

Figure 4.6: The total formation energies(in part (a)) and the cell constants (in part (b)), for the crystal structures with Parameter Set 2. The horizontal axes in both graphs represent the composition in the B-C-N trend

4.2.2 Random Phases Results

A random $4 \times 4 \times 4$ (512 atoms) and $7 \times 7 \times 7$ (2744 atoms) are considered. Tables 4.4, 4.8,and 4.9 show the properties obtained. Similarly, a dependance of these properties on the B-C-N composition is clearly shown in the figures 4.4, 4.7- 4.9.

Structure	Energy(Ev/atom)	C_{11}	C_{12}	C_{44}	B	G	ε	μ
BC	-6.8396	466.12	142	212	249.78	192	394	0.238
B_4C_3N	-6.4972	523	137	225	265	215	463	0.21
B_2CN	-6.195	527	135	360	290	264	577	0.171
B_4CN_3	-5.9639	747	106	355	320	341	721	0.123
BN	-5.8473	895	73	526	347	480	885	0.0755
$B_3C_2N_3$	-6.0470	862	105	459	357	427	840	0.108
BC_2N	-6.4275	849	113	522	368	451	884	0.112
BC_6N	-6.8965	971	102	564	392	512	951	0.0951
$Diamond(C_8)$	-7.3706	1074	102	642	426	579	1056	0.08651
BC_7	-7.2521	918	110	537	380	484	895	0.107
BC_3	-7.1224	767	120	429	334	387.3	728	0.135
B_3C_5	-6.9603	620	132	322	293	292	563	0.173
BC	-6.8396	466.12	142	212	249.78	192	394	0.238

Table 4.8: Properties of random, 2744 atoms, phase of B-C-N structures. The Elastic properties are expressed in units of GPa. Energy refers to the total formation energy.

Structure	a_1(Å)	a_2(Å)	α^0	β^0	γ^0
BC	3.644	3.644	90	89.95	90.07
B_4C_3N	3.627	3.627	89.99	90.07	89.97
B_2CN	3.615	3.615	90.06	90	90.04
B_4CN_3	3.61	3.61	89.98	90	90.05
BN	3.62(3.617)^a	3.62(3.617)^a	90	90	90
$B_3C_2N_3$	3.58	3.583	89.96	90.02	89.99
BC_2N	3.57(3.602)^a, (3.64)^b	3.57(3.602)^a, (3.64)^b	90.07	90	90.01
BC_6N	3.567	3.566	89.98	89.98	89.98
$Diamond(C_8)$	3.57	3.57	90	90	90
BC_7	3.585	3.585	90	90	89.99
BC_3	3.6038	3.604	89.99	90.01	90
B_3C_5	3.623	3.623	89.98	89.99	90.01
BC	3.644	3.644	90	89.95	90.07

(a) Reference[101]

(b) Reference[55]

Table 4.9: Properties of, 2744 atoms, random, phase of B-C-N structures, using Parameter set 2. Values in brackets are experimental values

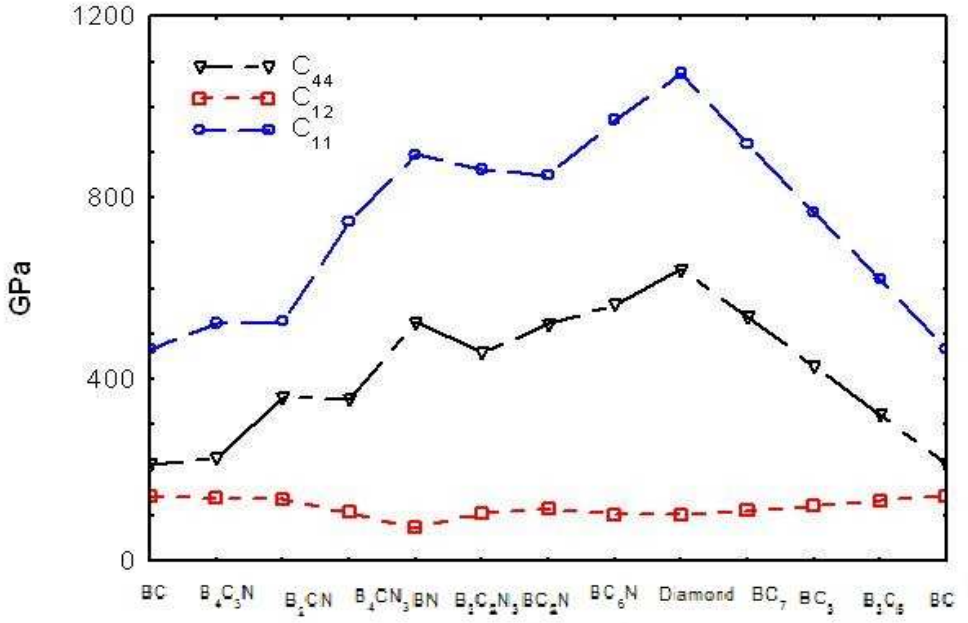

(a)

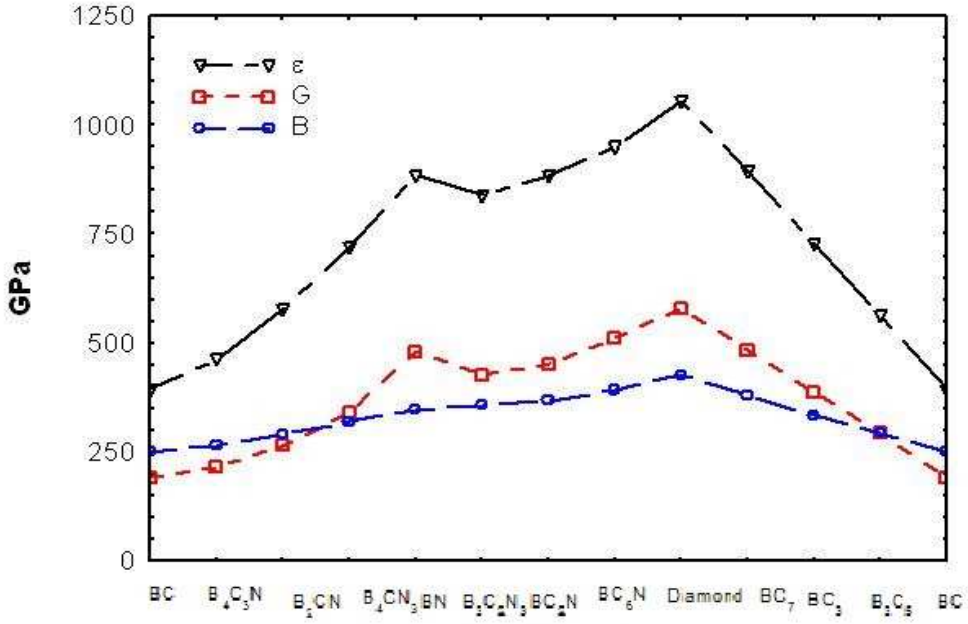

(b)

Figure 4.7: The elastic constants (shown in part (a), and the Moduli (shown in part (b)) for the 2744 atoms, random structure, using Set 2. The horizontal axes represent the B-C-N composition

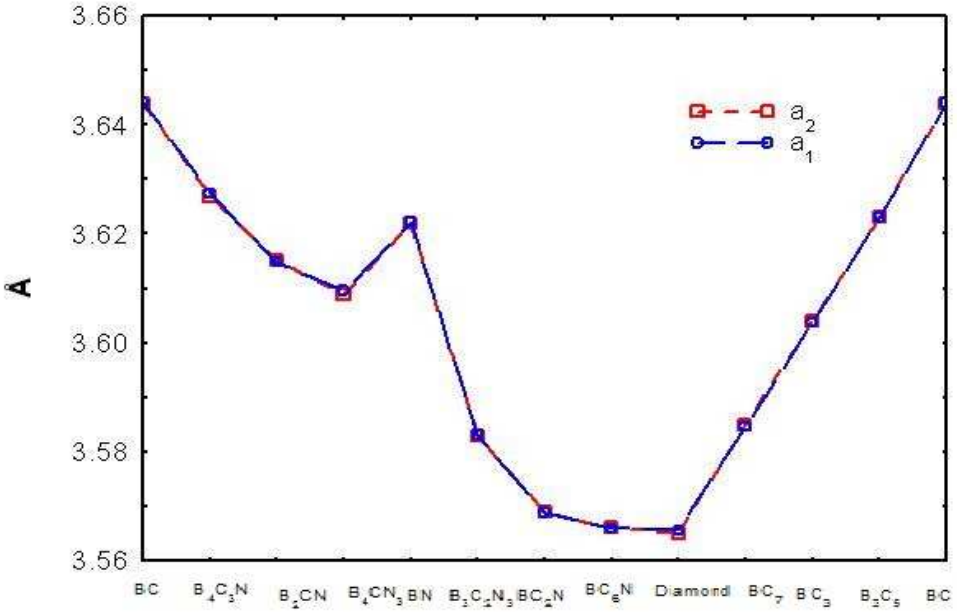

(a)

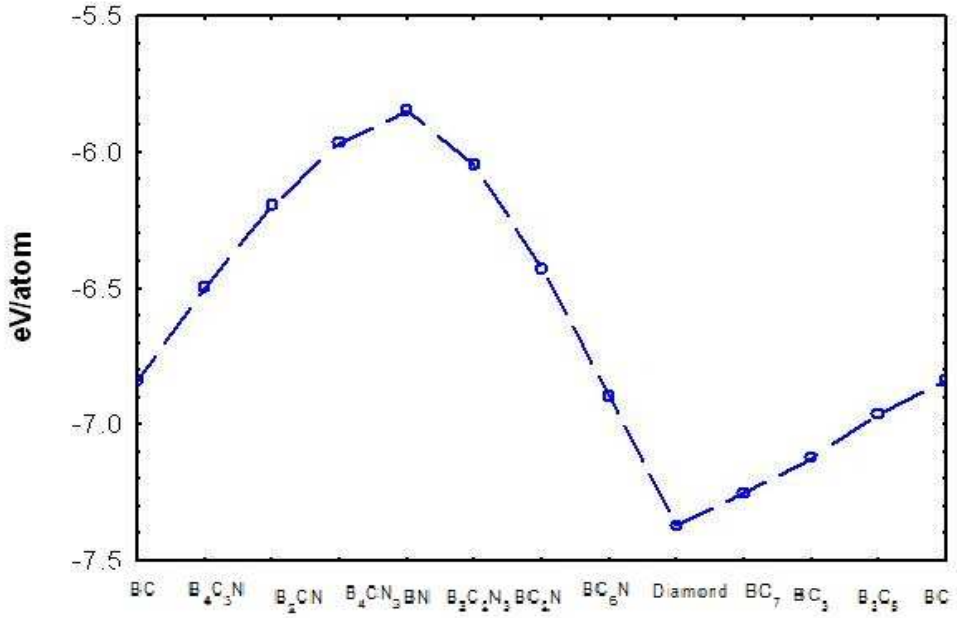

(a)

Figure 4.8: Total energy (in part (a)) and cell constants for the random, structures, with 2744 atoms, using Set 2, plotted against the B-C-N composition.

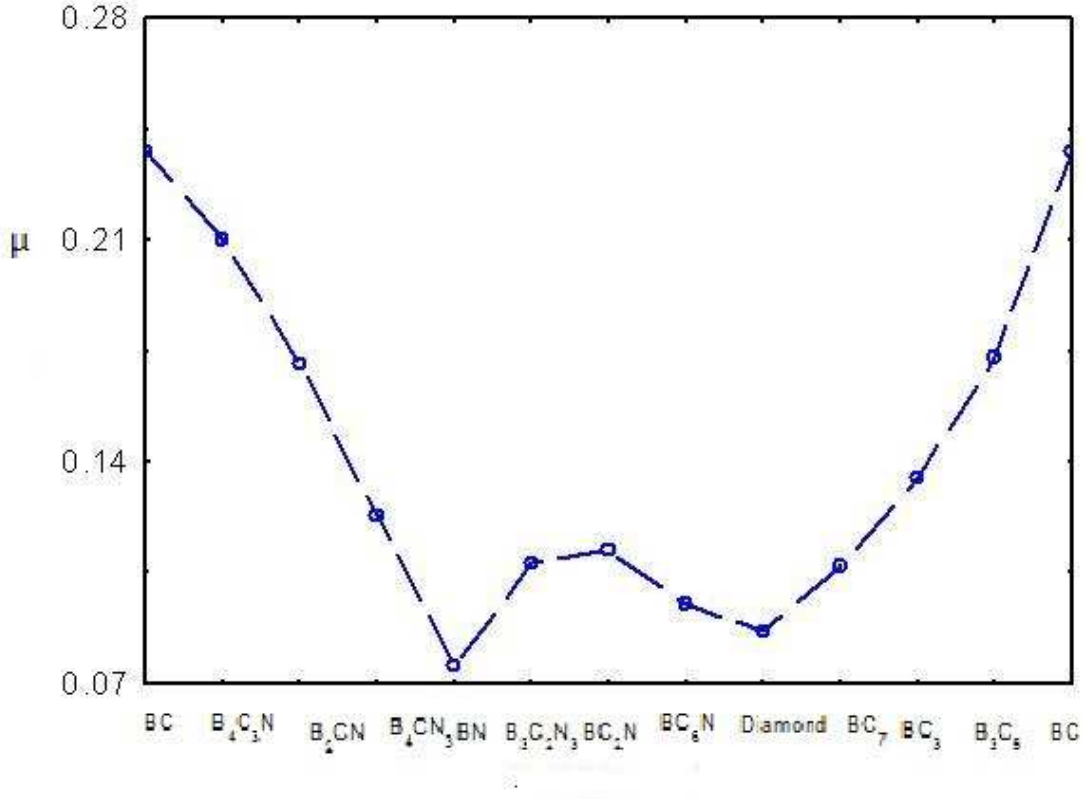

Figure 4.9: Poisson ratio μ against the B-C-N composition.

A graph illustrating the percentage number of bonds against the B-C-N trend is plotted as shown in figure 4.10. Here the horizontal axes are showing the percentage of each type of bond to the total number of bonds in the structure.

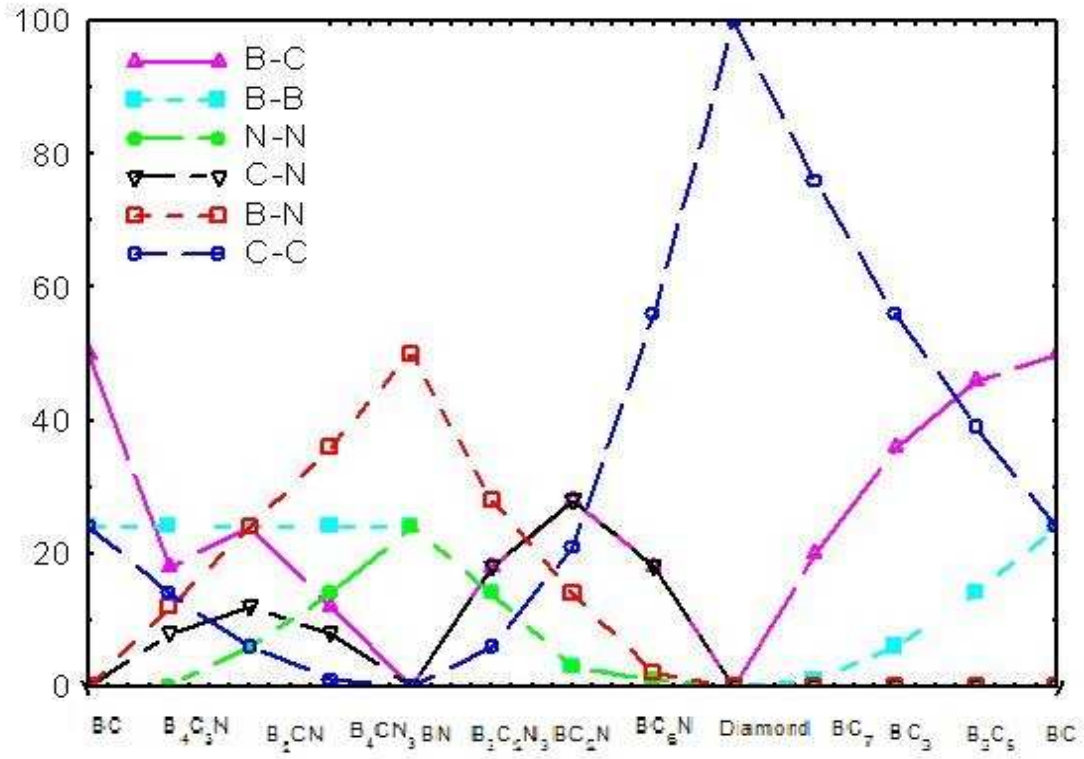

Figure 4.10: Percentage number of bonds against the B-C-N composition

Chapter 5

Discussion and Conclusion

The B-C and B-C-N materials have been studied using Tersoff potentials applied in the GULP code. The calculated formation energies, elastic constants and moduli were compared with the available results for diamond, BN and BC_2N . We found a good agreement of the calculated results with experiments[96] for the Bulk modulus and elastic constants but a slight discrepancy in the total energy . We found the cell constant for diamond to be 3.565 Å which is very close to the experimental value of 3.567 Å by Tiedje *et al*[95]. There is a 1.6 % difference between the experimental value of the bulk modulus of diamond by Mayer *et al*[96] and our calculated value of 425 GPa. Amongst the BC_3 structures, the tetragonal structures show better stability,

as evident from lower formation energy than found for trigonal phase.

To our knowledge there are no experimental results for the other B-C and B-C-N stuctures and hence our studied materials are novel.

To gain a further insight into the results graphs are plotted as shown in figures 3.2-3.12, 4.3- 4.10. This is mainly done to show the dependence of various properties of these materials on the concentration of B, C or N. All our structures show large values for elastic constants, especially the C_{11} and C_{44} components. Large Moduli values, especially Young's modulus and the bulk modulus which is a reciprocal of compressibility. The bulk modulus can be used as an indication of the materials' strength, chemical bonding and electronic structure[102]. This is somewhat an indication of an ultra-incompressible and superhard material. This work has also indicated that similar trends in the behaviour of the bulk, shear and elastic moduli of diamond-like B-C and B-C-N structures are deduced from the Tersoff potential calculations.

It is of importance that the size of the chosen supercell for the randomization process does not affect the final result or the choice of numerical

randomization. This, is ascertained by varying the supercell size to assure convergence. Employing structural optimisation ensures better quality of the starting structure[10]. We note the convergence of the moduli is quite rapid as illustrated graphically by figure 3.10. Amongst the B-C-N structures we only have considered an 8 atoms supercell. This is done because there is not much change in the structure even if it was bigger, since the atoms are fixed in their lattice positions.

As expected , randomization does not have any effect on the results for diamond, since all lattice points contain identical carbon atoms. This is clearly seen in figure 3.11, with energy differences very close to zero and in figure 3.12, where the ratio of cell constants is very close to 1.

It is of interest that the results, especially BC_2N results are closer to *ab initio* results by Sun *et al*[58]. The calculated value for bulk modulus for BC_7 of $377 - 382$ GPa is close to the value of 387 GPa obtained by first principles calculation recently done by Liang *et al*[103].

Two sets of nitrogen Tersoff parameters have reported in literature by Matsunaga *et al*[72](Set 1) and Justo *et al*[73](Set 2), and we have used

these parameter sets for simulation. Very good results were obtained using nitrogen parameter Set 2, whereas Set 1 parameters for nitrogen yielded poorer results, as they seem to be unphysical. Thereafter, B-C-N properties were only studied using Set 2 parameters. There is a good agreement for our calculated results for BN and BC_2N with experimental results found in the literature [55, 101, 18]. Amongst the BC_3 structures, the tetragonal structures are observed to have a lower formation energy than the trigonal structures.

In conclusion we have successfully used the empirical Tersoff interatomic potentials, applied in the Gulp code, to simulate 13 different diamond-like structures and have determined a number of structural properties. The Gulp molecular dynamics code yielded very good results for B-C and B-C-N materials. The fitted Tersoff interatomic potentials give very good results for diamond in comparison with experiment.

We have studied the mechanical properties and formation energies of B-C and B-C-N structures. The values obtained for the B-C and B-C-N structures confirm that they are superhard materials with hardness comparable, though slightly lower, to that of diamond. They are promising hard materials with

very interesting properties which may even work when diamond fails, since they have a different chemical and electrical properties from diamond.

The Tersoff parameters for nitrogen reported by Matsunaga *et al*[72] do not give desirable results in this work, in the sense that the properties obtained are unphysical. Hence we can conclude that they are not suitable for B-C-N materials. Since use of the parameter Set 2 nitrogen reported by Justo *et al*[73] yielded very good results, they were acceptable for B-C-N modelling materials. Experimental values for the lattice constant($3.635 \pm 0.006\mathring{A}$) and bulk modulus($335 \pm 8GPa$) of BC_5[23] are closer to our calculated values for trigonal BC_3.

The bulk modulus of the B-C materials increases as then number of boron-carbon bonds decreases and the number of carbon-carbon bonds increases. This is expected since there is a weaker bonding between B and C bonds in comparison to the C-C bonding. The experimental values for lattice parameter and bulk modulus of BC_5[16] are closer to our calculated values for trigonal BC_3. Relative to diamond and boron, it is expected that these structures should be metastable, as seen in previous results[18]. In addition the B-C structures are lighter than diamond and may shape more easily than

diamond. With regard to Poisson ratio, elastic constants and moduli, BC_6N is second in hardness after diamond.

With the exceptional hardness, implied by the high elastic constants, especially C_{44}, and the high moduli values, the B-C and B-C-N materials are attractive alternatives for advanced abrasives and high-temperature electronics. Since boron is a metalloid which implies intermediate conductivity, we expect the B-C materials to make good semiconductors. Further since boron has a lower atomic mass than Carbon, hence we anticipate the B-C materials to be lighter than diamond. In addition the atomic radius of N is smaller than that of C, hence substitutional of N atoms for C atoms is expected to result in significant strain in diamond crystal. The pair of nitrogen and boron should be the perfect co-doping candidates for making a n-type diamond-like material.

This work could be furthered by looking into the electronic structure of such materials, using *ab initio* molecular dynamics codes. The electronic structure is of interest since it may reveal some further important properties of these novel materials, such as their use for jewellery which is of great importance in life.

Bibliography

[1] K.Cornelis H.Cornelius. *Manual of Mineralogy*. Wiley, 20th edition, 1985.

[2] T. Forester W. Smith and I. Todorov. *The DL POLY_ 2 Uer Manual*. STFC Daresbury Laboratory, 2008.

[3] R. Garg I. Drouzas J. Ulloa P. Koenraad M. Steer H. Liu M. Hopkinson D. Mowbray V. Haxha, M. Migliorato. The use of abel-tersoff potentials in atomistic simulations of InGaAsSb/GaAs. Online at http://www.nusod.org/conf08/ThA4.pdf, September 2008.

[4] C. Kittel. *Introduction to Solid State Physics*. Wiley, 6th edition, 1996.

[5] Online at http://www.gordonengland.co.uk.

[6] R.L. Smith G.E. Sandland, editor. *An Accurate Method of Determining Hardness of Metals, With Particular Reference to Those of High Degree of Hardness,*. Institute of Mechanical Engineers, 1922.

[7] Hardness testing -the test methodology guide, part-2. online at www.hardnesstesters.com/hardness-method-2.htm, 2008.

[8] M. Allen. *Comp.Soft Matter*, 23, 2004.

[9] M. L.Cohen. *Phys.Rev.B*, 32:12, 1985.

[10] J. Gale. *General Utility Lattice Program 3.1.* Nanochemistry Research Institute, Department of Applied Chemistry, Curtin University of Technology,.

[11] F. Birch. *Phys.Rev.*, 71:908, 1947.

[12] M. Hebbache. *Solid state Comm.*, 113:427–432, 2000.

[13] Online at http://www.engineeringtoolbox.com.

[14] A. Schmidt O. Boresi and R. Sidebottom. *Advanced Mechanics of Materials,*. Wiley, 1993.

[15] E.Ziambaras and E. Schröder. *Phys.Rev. B*, 68:064118, 2003.

[16] V. Solozhenko, O.Kurakevych, D. Andrault, Y. Le Godec and M. Mezouar. *Phys.Rev.Lett.*, 102:015506, 2009.

[17] G. T. Gao, K. Van Workum, J. D. Schall and J. A. Harrison. *J.Phys.Cond.Matter*, 18:S1737–S1750, 2006.

[18] R.Hemley V.Brazhkin, A.Lyapin. *Philosophical Magazine A*, 82(2):231–253, 2002.

[19] H-Y. Chung. *Science*, 316:436, 2007.

[20] J. E. Lowther. *J.Phys.Cond.Matter*, 17:3221–3229, 2005.

[21] R. Crenko. *Phys.Rev.B.*, 7(10), 1973.

[22] J. Custers. *Nature*, 176:173–174, 1955.

[23] V.Solozhenko, N.Dubrovinskaia, L.Dubrovinsky. *Appl.Phys.Letters*, 85:1508, 2004.

[24] S. Louie M. Cohen S. Han, J. Ihm. *Phys. Rev. Lett.*, 80:995, 1998.

[25] A. Collins A. Williams, E. Lightowlers. *J. Phys. Condens. matter*, 3:1727, 1970.

[26] A. Collins A. Williams. *J. Phys. Condens. Matter*, 4:1789, 1971.

[27] R. Chrenko B. Massarani, J. Bourgoin. *Phys. Rev. B*, 17:1758, 1978.

[28] R. Mamin and T. Inushima. *Phys. Rev. B*, 63:033201, 2001.

[29] I. Snook A. Barnard, S. Russo. *J, Chem. Phys.*, 118:10725, 2003.

[30] W. Wilson. *Phys.Rev.*, 127:1549, 1962.

[31] H.Sagai K.Haruna H.Maeta N.Matsumoto T.Sato, K.Ohashi and H.Otsuka. *Phys.Rev.B*, 61:12970, 2001.

[32] E. Bauer N. Mel'nik N. Curro J. Thompson S. Stishov E. Ekimov, V. Sidorov. *Nature*, 428:542, 2001.

[33] S. Sque R. Jones J.Goss, P. Briddon. *Phys. Rev. B*, 69:165215, 2004.

[34] A. Voronov and A. V. Rakhmanina. *Inorg. Mater*, 29:707, 1993.

[35] V. Torishni A. Vishnevski, A. Gontar and A. A. Shulzhenko. *Sov. Phys. Semicond.*, 15:659, 1981.

[36] A. Deneuville F. Fontaine L. Abello P. Gonon, E. Gheeraert and G. Lucazeau. *J.Appl.Phys.*, 78:7059, 1995.

[37] P. Germi M. Pernet F. Brunet, A. Deneuville and E. Gheeraert. *J. appl.Phys.*, 81:1120, 1997.

[38] H. U. Baerwind E. Obermeier L. Haase W. Seifert A. Ringhandt C. Johnston S. Romani H. Bishop M. Werner, O. Dorsch and P. Chalker. *Appl. Phys. Lett.*, 64:595, 1994.

[39] E. Gheeraert E. Bustarret and K. Watanabe. *Phys. Stat. Solidi A*, 199:9, 2003.

[40] E. Bauer N. Melnik N. Curro J. Thompson E. Ekimov, V. Sidorov and S. Stishov. *Nature (London)*, 428:542, 2004.

[41] Yu. A. Timofeev A. Utyuzh and A. Rakhmanina. *Inorg. Mater.*, 40:926, 2004.

[42] M. McCluskey M. Plano J. Ager III, W. Walukiewicz and M. Landstrass. *Appl. Phys. Lett*, 66:616, 1995.

[43] C. Marcenat E. Gheeraert C. Cytermann J. Marcus E. Bustarret, J. Kaèmarèik and T. Klein. *Phys. Rev. Lett.*, 93:237005, 2004.

[44] L. Cohen A. Liu, M. Wentzcovitch. *Phys.Rev. B*, 39:3, 1989.

[45] D. Roundy M. Cohen S.Louie H. Sun, S. Jhi. *Phys. Rev. B*, 64, 2001.

[46] A.Lyapin S. Popova A.Rakhmanina S. Stishov V. Lebedev Y. Katayama V.Brazhkin, E.Ekimov and K. Kato. *Phys.Rev.B*, 74(R):140502, 2006.

[47] S.Louie M.Cohen S.Han, J.Ihm. *Phys.Rev.Lett.*, 80:5, 1998.

[48] R. Farrer. *Solid State Comm.*, 7:685, 1969.

[49] A. Badzian. *Mater. Res .Bull*, 16:1385, 1981.

[50] M. Hubacek and T. Sato. *J. Solid State Chem.*, 114:258, 1995.

[51] V.Turkevich V. Solozhenko and T. Sato. *J. Am. Ceram. Soc.*, 80:3229, 1997.

[52] Y. Zhao. *J. Mater. Res*, 17:3139, 2002.

[53] B. Xu Q. Wu Q. Hu Z. Liu J. He D. Yu Y. Tian H. Wang X. Luo, X. Guo. *Phys.Rev. B*, 76(094103), 2007.

[54] L. Daemen T.Shen R. Schwarz Y. Zhu D.Bish J. Huang J. Zhang G. Shen J. Qian Y. Zhao, D. He and T. Zerda. *J. Mater. Res*, 17:3139, 2002.

[55] G. Fiquet M. Mezouar V. Solozhenko, D. Andrault and D. Rubie. *Appl. Phys. Lett.*, 78:1385, 2001.

[56] P. Zinin M. Manghnani S. Tkachev, V. Solozhenko and L. Ming. *Phys.Rev.B*, 68:052104, 2003.

[57] M. Gubachek N. Borimchuk V. Zelyavskii N. Ostrovskaya V. Yarosh .V. Kurdyumov, V. Solozhenko. *Powder Metall. Met. Ceram.*, 93:629–637, 2000.

[58] Y-X. Fan J. Chen H-T. Wang X. Guo J. He J. Sun, X-F. Zhou and Y. Tian. *Phys.Rev.B.*, 73:045108, 2006.

[59] S. Azevado and R.De Paira. *Euro.Phys.Lett.*, 75:126, 2006.

[60] J. Tersoff. *Phys.Rev.lett.*, 61(25), 1988.

[61] J.Tersoff. *Phys.Rev. B*, 39(8), 1989.

[62] A. Hinchliffe. *Molecular Modelling for Beginners.* Wiley, 2003.

[63] J. Ogivile. *Dynamic Aspects of Intermolecular Interactions*, chapter 5, pages 49–56. Plenum Press, New York, 1998.

[64] M.Z. Bazant. *Interatomic Forces in Covalent Solids.* PhD thesis, Department of physics, Havard university , Cambridge Massachusetts, July 1997.

[65] J. Gale. *J. Chem. Soc., Faraday Trans.*, 1:629, 1997.

[66] M. Gillan W. Smith, G.N. Greaves. *J. Chem. Phys.*, 3091, 1995.

[67] D. Saada. *Comparison between Tersoff Potential and ab initio results for Surface Graphitazation of Diamond.* PhD thesis, Technion, Israel Institute of Technology, Department of Physics, 2000.

[68] J.Tersoff. *Phys.Rev.B*, 37(12), 1988.

[69] Furio Ercolessi. A molecular dynamics primer. International School for Advanced Studies, Trieste, Italy, 1997.

[70] J. Justo F. de Brito Mota and A. Fazzio. *Phys.Rev. B*, 58(13), 1998.

[71] D. Brenner. *Phys.Rev.B*, 42(15), 1990.

[72] K. Matsunaga, C. Fisher and H. Matsara. *Japan J. Appl. Phys.*, 39:L41, 2000.

[73] A. Fazzio F. de Brito Mota, J.F. Justo. *J.Int. Quantum Chem.*, 70:973, 1998.

[74] Ho J. Hwang W. Ha Moon. *Phys.Lett. A*, 315:319–324, 2003.

[75] D. Rachedb K. Amaraa, B. Soudinib and A. Boudalia. *Comp.Mater.Sci.*, 44(2):635–640, 2008.

[76] P. Erhart J. Nord, K. Albe and K. Nordlund. *J. Phys.Cond. Matter*, 15:5649–5662, 2003.

[77] J. Haile. *Molecular Dynamics Simulation, Elementary Methods*. Wiley Interscience, 1992.

[78] J.R. Beeler Jr. and G.L. Kulcinski. Agenda discussion:computer techniques. In J.R. Beeler Jr. P.C. Gehlen and R.I. Jaffe, editors, *Interatomic Potentials and Simulation of Lattice Defects*, pages 735–751. Plenum Press, 1972.

[79] C. Lubich E. Hairer and Gerhard Wanner. *Acta Numerica.*, 12:399–450, 2003.

[80] B. J. Alder and T. E. Wainwright. *J. Chem. Phys*, 31(459), 1959.

[81] W. Vetterling and B. P. Flannery W. Press, S. Teukolsky. *Numerical Recipes*. Cambridge University Press,, 2nd edition, 1992.

[82] Mark E. Tuckerman and Bruce J. Berne. Molecular dynamics algorithm for multiple time scales: Systems with long range forces. *J.Chem Phys.*, 94(10), 1991.

[83] M.Born and R.Oppenheimer. *Ann. Physik*, 84(457), 1927.

[84] J. Furthmuller G.Kresse, M. Marsman. *VASP the GUIDE*, 2009.

[85] Online at http://www. castep.org.

[86] Online at http://www.univie.ac.at/newtonx.

[87] C. Bayly I. Gould K. Merz D. Ferguson D. Spellmeyer T. Fox J. Caldwell W. Cornell, P. Cieplak and P. Kollman. *J. Am. Chem. Soc.*, 117:5179–5197, 1995.

[88] A. Gursoy A. Dalke L. Kale R. Skeel K. Schulten M. Nelson, W. Humphrey. Namd- a parrallel, object -oriented molecular dynamics program. 1996.

[89] B.Olafson D. States S. Swaminathan B. Brooks, R. Bruccoleri and M. Karplus. *J. Comp. Chem*, 4:187–217, 1983.

[90] D. Burnett. *Finite Element Analysis: From Concepts To Applications*. Addison-Wesley, 1987.

[91] L. Verlet. *Phys. Rev*, 159(98), 1967.

[92] A. Rahman. *Phys. Rev*, 136(405), 1964.

[93] B. Montgomery Pettitt Paul E. Smith. Efficient ewald electrostatic calculations for large systems. *Comp. Phys. Comm.*, 91:339–344, 1995.

[94] D.Chung and W.Buessem. *J. Appl.Phys.*, 39(2777), 1968.

[95] T. Tiedje K. Myrtle M. Kasrai J.R. Dahn, B.M. Way. *Phys.Rev.B*, 46:1697, 1992.

[96] L. Mayer Y. Baskin. *Phys.Rev.*, 100:44, 1955.

[97] D. Roundy M. Cohen S. Louie S. Jhi, H. Sun. *Phys.Rev.B*, 64:755, 2008.

[98] A. Pollan E. Zouboulis, M. Grimsdditch. *J. Appl.Phys.*, 76(882), 1994.

[99] S.Kim L.Kleinman D.Bylander, S.Lee. *Phys.Rev.B*, 45:3248, 1992.

[100] D. Andrault Y. Le Godec V. Solozhenko, O. Kurakevych and M. Mezouar. *Phys.Rev.Lett.*, 102:015506, 2009.

[101] R. Jeanloz E. Knittle, R. Kanner and M.L. Cohen. *Phys.Rev. B*, 51(18), 1995.

[102] C. Yoo H. Cynn, J. Klepeis and D. Young. *Phys.Rev. Lett.*, 88(13), 2002.

[103] J. Zhao Y. Liang, W. Zhang and L. Chen. *Phys.Rev.B*, 80(113401), 2009.